Lab on a Chip

CRITICAL REVIEW

View Article Online
View Journal | View Issue

CrossMark click for updates

Cite this: *Lab Chip*, 2017, **17**, 751

Active droplet sorting in microfluidics: a review

Heng-Dong Xi,†[a] Hao Zheng,†[a] Wei Guo,[ah] Alfonso M. Gañán-Calvo,[b] Ye Ai,[c] Chia-Wen Tsao,[d] Jun Zhou,[e] Weihua Li,[f] Yanyi Huang,[g] Nam-Trung Nguyen[h] and Say Hwa Tan*[h]

Received 21st November 2016, Accepted 2nd February 2017

DOI: 10.1039/c6lc01435f

rsc.li/loc

The ability to manipulate and sort droplets is a fundamental issue in droplet-based microfluidics. Various lab-on-a-chip applications can only be realized if droplets are systematically categorized and sorted. These micron-sized droplets act as ideal reactors which compartmentalize different biological and chemical reagents. Array processing of these droplets hinges on the competence of the sorting and integration into the fluidic system. Recent technological advances only allow droplets to be actively sorted at the rate of kilohertz or less. In this review, we present state-of-the-art technologies which are implemented to efficiently sort droplets. We classify the concepts according to the type of energy implemented into the system. We also discuss various key issues and provide insights into various systems.

[a] *School of Aeronautics, Northwestern Polytechnical University, 127 West Youyi Rd., Xi'an, Shaanxi, China*
[b] *Depto. de Ingeniería Aeroespacial y Mecánica de Fluidos, Universidad de Sevilla, E-41092 Sevilla, Spain*
[c] *Pillar of Engineering Product Development, Singapore University of Technology and Design, Singapore*
[d] *Department of Mechanical Engineering, National Central University, No. 300, Zhongda Rd, Taoyuan, Taiwan*
[e] *School of Information and Communication Technology, Griffith University, Nathan, QLD 4111, Australia*
[f] *School of Mechanical, Materials and Mechatronic Engineering, University of Wollongong, Wollongong, NSW 2522, Australia*
[g] *Biodynamic Optical Imaging Center, Peking University, Beijing 100871, China*
[h] *Queensland Micro- and Nanotechnology Centre, Griffith University, 170 Kessels Road, Brisbane, QLD 4111, Australia. E-mail: sayhwa.tan@griffith.edu.au*
† These authors contributed equally to this work.

1 Introduction

Microfluidics is the science and technology dealing with fluidic phenomena on the microscale. The small size of microfluidic devices reduces the amount of samples and reagents needed by several orders of magnitude. The initial approach in microfluidics research was scaling down conventional laboratory equipment and processes. Samples and reagents were delivered and manipulated by miniaturized pumps and valves integrated into the same device within a microchannel network. Typically, the significance of molecular diffusion grows relative to that of convective mass transfer with sample size reduction. Furthermore, the laminar flow regime in

Heng-Dong Xi

Heng-Dong Xi is a professor in the School of Aeronautics, Northwestern Polytechnical University, Xi'an, China. He received his Ph. D. degree from The Chinese University of Hong Kong in 2007. He was a postdoctoral fellow in Max Planck Institute for Dynamics and Self-Organization from 2009 to 2012. He was awarded the Humboldt Fellowship in 2010. He received the "1000-young Talent Program" of China in 2012 and worked as a professor in Shenzhen Graduate School, Harbin Institute of Technology. Since 2014, he has been a professor at Northwestern Polytechnical University. His research interests include microfluidics, thermal convection, polymeric drag reduction, and turbulence.

Hao Zheng

Hao Zheng received his bachelor's degree in Aircraft Design Engineering from Northwestern Polytechnical University, China in 2016. He is currently a master's student in the School of Aeronautics, Northwestern Polytechnical University, China. His research interest is focused on active droplet manipulation in microfluidics.

microchannels raises specific issues. Particularly, the laminar flow is stable and predictable but prevents efficient mixing in many applications.

Miniaturizing fluidic handling is usually associated with continuous-flow microfluidics.[1,2] Furthermore, when dealing with different molecularly immiscible fluid species and reagents, the corresponding surface tension at interfaces introduces surface forces that tend to reduce the contact area. Thus, surface tension makes continuous-flow microfluidics essentially unstable, driving the system to a discontinuous, often periodic flow where a phase forms droplets. This fundamental effect, together with geometrical constraints, leads to what is now called droplet-based microfluidics.[3] The fundamental advantage of droplet-based microfluidics is that a continuous stream of a fluid carrying samples is divided into very small volumes ranging from nanoliters to picoliters, *i.e.* microdroplets. The two major branches of droplet-based microfluidics are digital microfluidics and continuous-flow droplet-based microfluidics. Digital microfluidics[4,5] deals with the manipulation of discrete droplets. Common manipulation schemes are electrowetting and magnetic actuation. In continuous-flow droplet-based microfluidics, droplets are formed and manipulated within an immiscible carrier fluid in a continuous manner. In this review, we focus on this second branch which is in short referred to as droplet-based microfluidics.

Wei Guo

Wei Guo received his bachelor's degree in Aircraft Design Engineering from Northwestern Polytechnical University, China in 2015. He is currently a master's student in the School of Aeronautics, Northwestern Polytechnical University, China. His research interest is in the interaction between an electric field and droplets in microfluidics.

Alfonso M. Gañán-Calvo

Alfonso M. Gañán-Calvo is a professor and chair of Fluid Mechanics in the Department of Aerospace Engineering and Fluid Mechanics at the University of Seville, Spain. He is also president of Ingeniatrics Tec. S.L., Spain. He received his master's and PhD degrees from the same university in 1987 and 1989, respectively. He was a postdoctoral researcher at the University of Southern California and a visiting professor at the University of California, San Diego, USA. Dr Gañán-Calvo has published over 125 journal papers and filed more than 150 patents. He is a recipient of the National Prize of Research "Juan de la Cierva" of Spain, 2010 and has been a fellow of the American Physical Society since 2012.

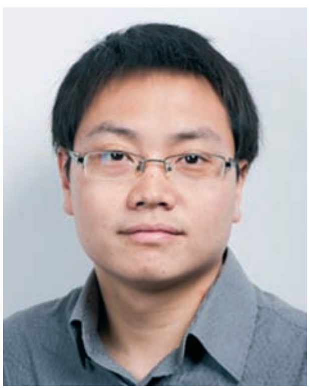

Ye Ai

Ye Ai has been an assistant professor at Singapore University of Technology and Design (SUTD) since 2013. He received his B.S. degree in Mechanical Engineering from Huazhong University of Science and Technology in 2005 and his Ph.D. degree in Mechanical and Aerospace Engineering from Old Dominion University in 2011. Prior to joining SUTD, he worked as a postdoctoral researcher at the Bioscience Division of Los Alamos National Laboratory. He was a visiting professor at Massachusetts Institute of Technology from August 2014 to July 2015. His research interest focuses on developing novel microfluidic technologies for microscale manipulation and single cell analysis.

Chia-Wen Tsao

Dr Chia-Wen Tsao is an associate professor in the Department of Mechanical Engineering, National Central University, Taiwan. He received his M.S. degree from the Department of Mechanical Engineering, University of Colorado at Boulder and his Ph.D. degree from the Department of Mechanical Engineering, University of Maryland at College Park. His research interests include micro/nano-fluidics, micro/nanofabrication, lab-on-a-chip devices, MEMS, and mass spectrometry technologies. He is the head of the Microfluidics and Microfabrication Laboratory, National Central University, Taiwan. Before joining the National Central University, he had four years of industrial experience working as a MEMS and mechanical engineer.

Droplet-based microfluidics allows for the generation and control of droplets in ideal microenvironments for a variety of chemical and biological applications and processes.[6,7] The large surface to volume ratio, short mixing distance and efficient mass and heat transfer within a droplet make the microdroplet a unique reactor platform. Furthermore, droplet-based microfluidics allows a large number of experiments to be performed and repeated in a single device, significantly improving the statistics of the results. Thus, the key functions in droplet-based microfluidic devices are the generation and manipulation of microdroplets. We recently reviewed the various active methods for droplet generation.[3]

After their generation, droplets move in microchannels in a continuous fashion. To fulfil specific functions and objectives, actuation technologies are needed for the manipulation of these droplets according to their contents. Basic manipulation tasks include droplet coalescence, mixing, sorting, and phase changing. In 2008, Teh *et al.*[8] provided an excellent review on general droplet manipulation procedures, technologies and applications of droplet-based microfluidics.

Jun Zhou

Jun Zhou received his B.S. degree in computer science and his B.E. degree in international business from Nanjing University of Science and Technology, Nanjing, China, in 1996 and 1998, respectively. He received his M.S. degree in computer science from Concordia University, Montreal, Canada, in 2002 and his Ph.D. degree from the University of Alberta, Edmonton, Canada, in 2006. He is a senior lecturer in the School of Information and Communication Technology at Griffith University, Nathan, Australia. His research interests include pattern recognition, computer vision and spectral imaging as well as their applications in remote sensing and environmental informatics.

Weihua Li

Weihua Li is a senior professor and director of the Advanced Manufacturing Research Strength at the University of Wollongong. He obtained his B. Eng. (1992) and M.Eng. (1995) degrees from the University of Science and Technology of China and his PhD degree from Nanyang Technological University, Singapore (2001). Since 2003, he has been working as part of the academic staff at the same school. His research focuses on smart materials, microfluidics, rheology, and intelligent mechatronics. He serves as a technical editor, an associate editor or an editorial board member for more than 10 international journals. He has published more than 300 journal papers. He is a recipient of the IOP Fellowship, Fellow of Engineers Australia, JSPS Invitation Fellowship and Australian Endeavour Fellowship (2011).

Yanyi Huang

Dr Yanyi Huang received his BS (Chemistry) and ScD (Inorganic Chemistry) degrees from Peking University in 1997 and 2002, respectively. He conducted his postdoctoral research at Caltech (Applied Physics, 2002–2005) with Amnon Yariv and at Stanford (Bioengineering, 2005–2006) with Stephen Quake. He started his independent career at Peking University in 2006 as a principal investigator and was then promoted to an associate professor in 2009 and a professor in 2013. He is a professor of materials science and engineering, a PI in Biodynamic Optical Imaging Center (BIOPIC), a PI in Peking-Tsinghua Center for Life Sciences, a PI in Beijing Advanced Innovation Center for Genomics, and an adjunct professor of analytical chemistry.

Nam-Trung Nguyen

Nam-Trung Nguyen is a professor and the director of Queensland Micro- and Nanotechnology Centre, Griffith University, Australia. He received his Dipl-Ing, Dr-Ing and Dr-Ing Habil degrees from the Chemnitz University of Technology, Germany, in 1993, 1997 and 2004, respectively. He was a postdoctoral research engineer at the Berkeley Sensor and Actuator Center, University of California, Berkeley, USA. From 1999 to 2013, he was a research fellow, an assistant professor and an associate professor at Nanyang Technological University, Singapore. Dr Nguyen has published over 280 journal papers and several books on microfluidics and nanofluidics.

Further advances have been made in the past eight years and the body of literature on droplet-based microfluidics has also grown significantly. However, to the best of our knowledge, no specific review on active droplet sorting exists. The present review focuses on the single task of droplet sorting for its unique significance. We limit the discussion to only water-in-oil droplets formed in a planar microfluidic system. The encapsulation of cells or particles in droplets and using a commercial flow cytometer are not discussed as the review seeks to focus on the different methods of active droplet sorting in microfluidics.

In a typical lab-on-a-chip application, particularly for biological analysis, samples are first prepared before the actual analysis. Sorting of cells and other biological particles are vital for the subsequent steps. In droplet-based microfluidics, these particles are encapsulated in a droplet. Thus, sorting of droplets based on its content is of immense significance for the subsequent analysis steps.

As sorting of droplets requires the discrimination of their properties, the first task in droplet sorting is droplet detection, which provides feedback to the actuator to sort droplets. In some concepts such as magnetic sorting, detection and sorting occur concurrently with the help of a permanent magnet. However, the detection in most sorting concepts requires a specific method to discriminate the size, content, and electric, magnetic and optical properties of droplets. Similar to the detection methods, active sorting can be categorized according to concepts such as electric, acoustic, magnetic, pneumatic and thermal actuation. As detection and actuation are often based on the same physical phenomenon, we focus on the latter to describe and elucidate the different active sorting mechanisms. Fig. 1 provides an overview of the different sorting concepts that are discussed in the following sections.

Say Hwa Tan

Dr Say Hwa Tan is an ARC DECRA fellow with Queensland Micro- and Nanotechnology Centre, Griffith University, Australia. He received his BEng, MEng and PhD degrees from Nanyang Technological University, Singapore and Georg-August-Universität Göttingen and Max Planck Institute for Dynamics and Self-Organization (MPI-DS), Germany, in 2008, 2010 and 2014, respectively. In 2016, he was highlighted as one of the 18 emerging investigators in the journal Lab on a Chip. Dr Tan has published more than 30 research works on microfluidics. His research has established and pioneered different approaches to manipulate droplets and bubbles using thermal, magnetic, acoustic and electric energies.

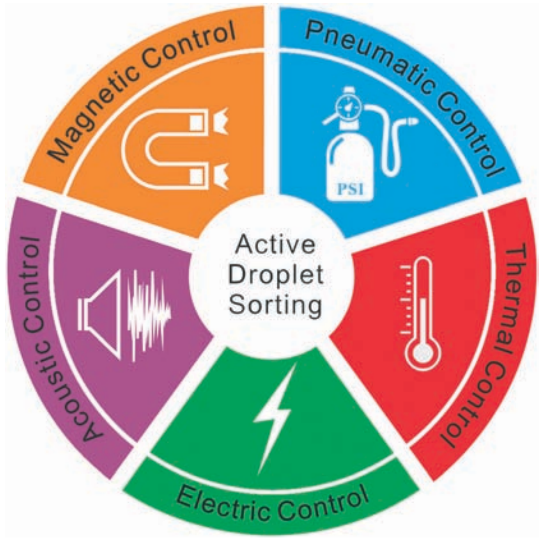

Fig. 1 Classification of different active droplet sorting methods.

2 Electric control

Droplet sorting by electrical means has undergone a dramatic development in the past decade. In contrast to passive sorting,[9–16] which is based on hydrodynamic features (*e.g.* size or shape sieving), these methods allow on-demand control using detectable electric features present in the droplet. Thus, high throughput and accuracy can be achieved with rapid electric detection and sorting. Although these methods are limited by the characteristic time scale of the physics and electrohydrodynamics involved, the time scale is generally below one millisecond and typically on the order of microseconds. In general, the use of electric forces to actuate the droplet dynamics demands the presence of sufficient free charges in the liquid droplet or sufficient differences in electric conductivities and/or electric permittivities between the carrier and dispersed liquid to create interfacial and/or bulk stresses on the droplets. This sometimes limits the degrees of freedom in the choice of liquids; however, the basic immiscibility requirement normally encompasses such electrochemical differences in most cases of interest.

Electric methods can be classified according to the type of current applied to the electrodes. In the following sections, we examine droplet sorting methods using either direct current (DC) or alternating current (AC) and describe their evolution in the respective applications.

2.1 Direct current

Link *et al.*[17] first employed a droplet sorting method using DC in 2006 (Fig. 2a). The microchannels were patterned in polydimethylsiloxane (PDMS) using soft lithography technology.[18,19] Two indium tin oxide (ITO) electrodes were placed on a glass surface facing the microchannels. The PDMS device was bonded to the glass slide assisted by oxygen plasma.[20] In the experiment, positively charged droplets flow into a T-junction bifurcation. Without an electric field, the

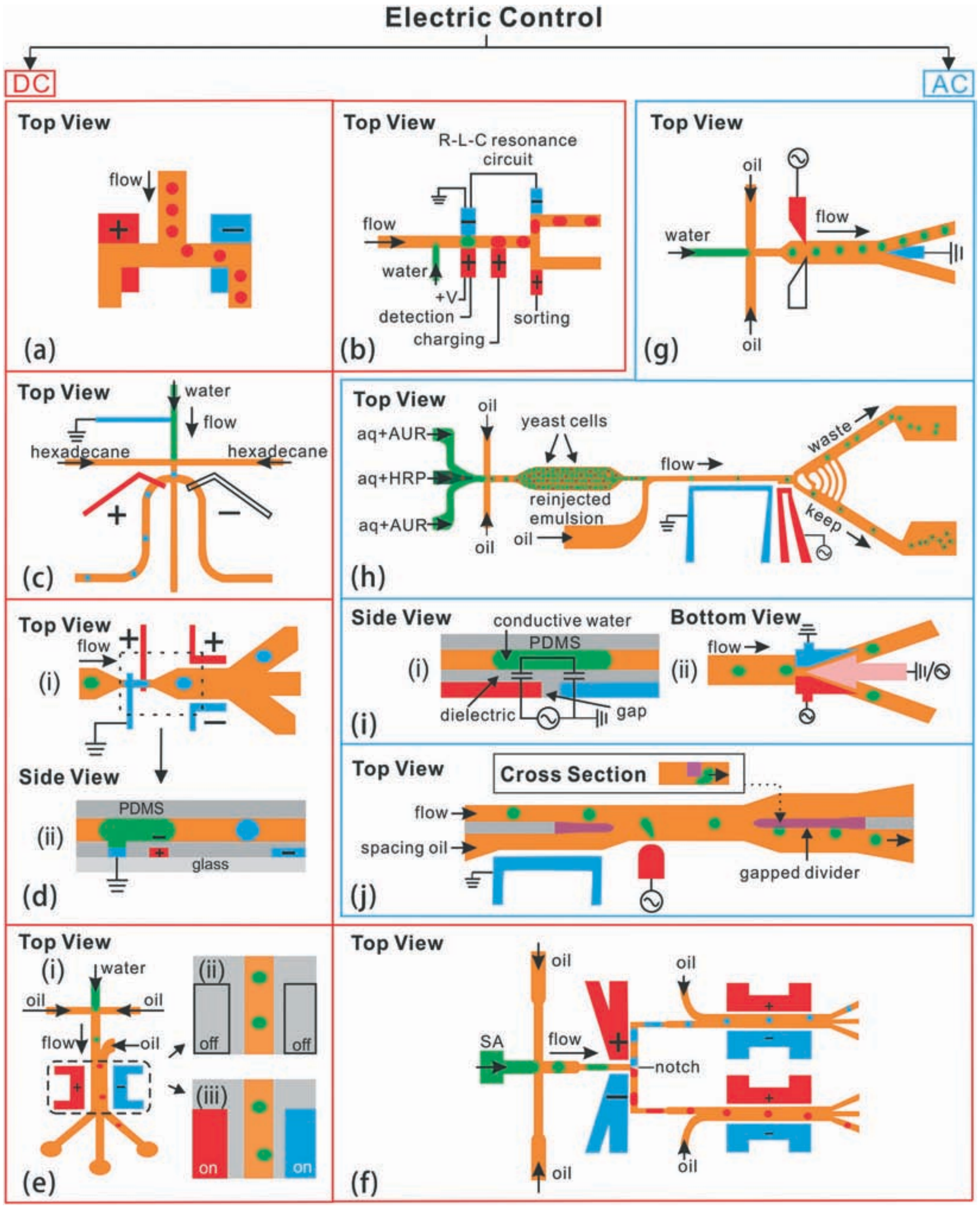

Fig. 2 Schematic sketches and classification of droplet sorting with electric methods. The orange and green parts represent oil and aqueous phases, respectively. The green droplets are electrically neutral, while the blue and red droplets are negatively and positively charged, respectively. For the DC/AC electric field, the red and blue electrodes represent positive and negative/grounded charging, respectively. Inactive electrodes are blank. (a) Positively charged droplets are sorted to the right branch; (b) three pairs of coplanar electrodes along the main flow channel for detection, charging and sorting. Droplets are positively charged and directed to the upper channel based on the detection results; (c) concurrent droplet charging for generation and sorting. Droplets are charged and directed to the left channel when the left positive electrode is actuated; (d) droplet pre-charging and sorting. (d-i) The droplet is first negatively charged by a pair of electrodes and then sorted to the upper channel. (d-ii) Side view for the negative charging procedure; (e) droplet self-charging and sorting. (e-i) Overview of the system. (e-ii) Without an electric field, droplets move along the central line and into the middle branch; (e-iii) with an electric field, droplets are "self-charged" and move to the negative side; (f) droplets are split into two oppositely charged daughter droplets and subsequently sorted in different sub-channels (SA: sodium alginate solution); (g) droplets flow to the upper channel when the upper electrode is energized; (h) droplets with yeast cells are sorted by dielectrophoresis into the bottom channel (aq: aqueous, AUR: Amplex Ultrared, HRP: horseradish peroxidase); (i) electrostatic potential well control. (i-i) Working principle of the electrostatic potential well. (i-ii) The middle electrode in pink has two states, grounded or actuated. When the pink electrode is grounded, droplets move to the lower branch. When it is actuated, droplets move to the upper branch; (j) ultrafast droplet sorting by DEP and by a gap divider. Droplets are deflected by DEP and squeezed into the lower branch by the gap divider.

droplets were randomly distributed between the two branches. To precisely control droplet actuation, a voltage V was applied between the two ITO electrodes, producing the electric field

$$E = V/d \tag{1}$$

and the electrostatic force on the charged droplet

$$F = qE \tag{2}$$

where d is the distance between the electrodes and q is the charge contained in the droplet. The electrostatic force F increases with field strength. If the field is sufficiently large, the electrostatic force drives the droplet with positive charge toward the negative electrode. Switching the polarization of the two electrodes can sort droplets into different channels.

However, this electric method requires droplets to be positively or negatively charged before they are sorted. One simple way to charge the droplet is by exposing it to an energized electrode as introduced by Niu *et al.*[21] (Fig. 2b). In their design, droplets are confined in the channel and in contact with the charging electrode before moving into the bifurcation. This gives positive charges on the droplet surface and allows these droplets to be sorted.

Another important contribution of this work is combining the sorting process with an AC detection method. The detection used an additional pair of electrodes before charging, which detected the capacitive changes caused by the passing-by droplets. As the contents of the droplets varied, the capacitive changes across the electrode were different and detectable. A computer program received the capacitance information and decided which branch the droplet should enter. The poles of the sorting electrodes were activated base on the result. This method allows a high sorting frequency of up to 10 kHz.

In 2009, Ahn *et al.*[22] introduced a method that combined both electric droplet generation and sorting (Fig. 2c). The central aqueous stream of a flow-focusing configuration is connected to the ground electrode for droplet generation. The other two electrodes are placed under two side branches and exposed to the flow. If both downstream electrodes are not energized, the generated droplets move directly to the centre branch. In the energized state, the left electrode for example is connected to a positive voltage, and the formed droplets become negatively charged at the orifice. The electrostatic force acting on the droplet competes against the interfacial tension, accelerating the droplet generation process.[17,23] After pinching off, the droplets carry negative charges, which are uniformly distributed on their surfaces. In this applied electric field, droplets are attracted to the positive electrode and sorted to the left channel (as shown in Fig. 2c), and *vice versa*. The benefit of this method is the short distance from droplet generation to sorting. However, it also has the disadvantage that droplet size depends on both the applied voltage and the flow rate of the two phases, which inevitably makes both control and operation difficult.

In 2011, the same group[24] introduced another pre-charging scheme using the induction effect (Fig. 2d). Droplets move into a small valve where they are confined by the top and bottom walls of the microchannel. Two coplanar indium tin oxide (ITO) electrodes are placed under the main flow channel at the valve. One electrode is grounded and exposed to the flow. The another electrode is either positively or negatively charged and separated from the channel by a thin PDMS wall. When the droplet passes through this valve, charges are induced on the water–oil interface. These charges are trapped and uniformly distributed across the surface of the droplet as it exits the valve and proceeded downstream. Thus, droplets could be sorted by the sign of the charges they carry by another pair of electrodes.

While it may be convenient to charge droplets by direct contact with the electrode, the drawbacks of this method are the possible electric short circuit and electrode fouling.

In 2010, Guo *et al.*[25] designed a sorting device using the so-called "droplet self-charging" phenomenon (Fig. 2e). Water-in-oil droplets are generated in a flow-focusing configuration and a sideway oil injection is used to adjust the distance between the two droplets. Two oppositely charged indium tin oxide (ITO) electrodes are placed alongside the main flow channel and generates an electric field across the channel, so that droplets are charged when they pass through this field. There has been no general consensus on the mechanism of this phenomenon. Possible explanations are induced charging or ion transformation between the aqueous droplet and the oil phase.[26–28] As a result, the droplets became positively charged and were deflected to the negative side. Thus, by switching the polarization of the two electrodes, droplets could be sorted into different branches.

Rao *et al.*[29] further improved this design by using one-step fabricated three dimensional (3D) silver paste electrodes. The electrodes are fabricated by injecting conductive silver paste into microchannels. Compared to the 2D counterparts, 3D electrodes could generate a stronger and more homogeneous electric field. It helps increase the deflecting velocity and reduce both the response and the recovery times for droplets deflecting and returning to the centre of the channel, respectively. Furthermore, the voltage needed to generate the electric field with 3D electrodes can be significantly reduced compared to the 2D model. The electrodes also don't require alignment as the microchannels were fabricated using the same lithography process.

Another sorting device introduced by the group[30] made use of 3D electrodes (Fig. 2f). In this design, a notch is used to split the original droplet, which is subjected to an electric field inducing opposite charges near its two hemisphere surfaces. The two daughter droplets then carry equal charges but with opposite signs and move into different channels. Subsequent sorting of the daughter droplets is based on the sign of the charges they have.

2.2 Alternating current

An AC electric field can be used in droplet manipulation such as generation,[31–34] deformation[35] and sorting. Ahn *et al.*[36] first reported the use of dielectrophoresis (DEP) for droplet sorting in 2006 (Fig. 2g). Dielectrophoresis (DEP) is the migration of a particle caused by dielectric force which is exerted on it in a non-uniform electric field.[37,38] The force is given by

$$\vec{F} = \vec{m}\cdot\nabla\vec{E} \tag{3}$$

where $\vec{m}$ is the dipole moment of the particle and $\vec{E}$ is the electric field. Droplets containing particles were generated from a flow focusing channel, and a Y-junction was used for sorting. Three electrodes were placed below the fluidic channel. One electrode was grounded and located in the centre of the bifurcation. The other two were placed so that their edges were near the centre line of the channel. The electrodes were triangular in shape in order to generate the largest field gradients. Without an electric field, the droplets were evenly distributed into both branches. However, if one upstream electrode was energized, the droplets were deflected to the same side of that electrode and moved into the corresponding sorting channel. Thus, droplet sorting could be realized by energizing different upstream electrodes.

A similar use of DEP can be found in the studies of Baret *et al.*[6] and Agresti *et al.*[39] (Fig. 2h). A bifurcation configuration sorted droplets with biological content such as yeast cells. In this method, one branch has a lower hydrodynamic resistance than the other so that, when there is no electric field, droplets flow into the branch with a lower resistance (the upper branch in Fig. 2h).[40–53] The electrode near the bifurcation is energized to pick up the droplets with a single cell inside. DEP force steers the droplets into the collecting channel (the lower branch in Fig. 2h). Interestingly, inverting the polarity of the electrodes results in the production of charged droplets. This could also result in droplet merging at the collection channel if the droplets are in contact with each other.

De Ruiter *et al.*[54] reported an electrowetting-on-dielectric (EWOD)[55,56] sorting method in 2014 (Fig. 2i). As shown in Fig. 2i-i, the electrically conducting droplet confined in the channel moves above the two co-planar electrodes. The electrodes are isolated by a thin PDMS film which acts as a dielectric layer. If an AC voltage is applied on the two electrodes, the droplet forms a closed circuit. The corresponding electric force is directed downward and traps the droplet in the gap between the electrodes. Optimising the oil flow rate, the voltage and the gap design (such as angled gap) could guide droplets along the gap and sort them at the channel outlet. Fig. 2i-ii shows that switching the centre electrode to an AC voltage or to the ground can sort droplets to the upper and lower branches, respectively. The initial sorting rate of this device is about 100 drops per second. Pit *et al.*[57] used an oil with a lower viscosity and a smaller opening angle and increase the sorting rate up to 1200 drops per second.

Sciambi *et al.*[58–60] developed an ultra high-speed droplet sorter utilizing DEP and a special channel geometry called gap divider (Fig. 2j). The gapped divider is a thin wall with one end attached to the channel ceiling and the other end 11 μm away from the channel floor. The divider along the centre line separates the channel into two equal parts. Neutral droplets enter the sorting region loosely constrained by a short gapped divider. A spacing oil flow confines the droplets to the channel side away from the electrode. The energized electrode attracts the droplet and slightly moves it to one side. The droplet then moves downstream to a longer divider with part of it squeezed by the gap. Due to this change, the small lateral displacement by DEP will increase as the droplet travels downstream and force the droplet into the predesigned channel, while the non-attracted droplets will be restrained to the other side. Since the first displacement by the electrode is small, the operating time needed for one droplet is relatively short. This results in an ultrafast sorting speed with the highest rate ever reported of approximately 30 kHz. While most droplets could be correctly sorted, certain errors may arise. First, a regular spacing is crucial to the sorting process. High flow speed would cause the droplet to stack vertically in multiple layers and lead to an irregular spacing. Thus, a two-layer inlet structure with the filter in the same shallow layer as the gapped divider is used to force droplets into a monolayer line. Second, droplets with an abnormally large or small size would fail in sorting. Monodisperse droplets are required for higher accuracy. One possible way to improve the sorting accuracy could be filtration of the emulsion.

3 Acoustic control

Acoustic control is an attractive technique for droplet manipulation and sorting due to its good biocompatibility. Biological samples such as cells can be encapsulated in droplets, retaining a high viability even with many hours of exposure to acoustic fields. Acoustic waves are generated mainly by piezoelectric actuators.[61] Two different wave modes are often exploited for droplet sorting. The first mode is surface acoustic wave (SAW),[62,63] a wave traveling along the surface of the substrate with an amplitude that decays exponentially along the normal direction of the substrate. The second mode is bulk acoustic wave (BAW),[64] which typically propagates through the medium rather than the surface. Interactions between propagating sound waves and the medium may give rise to two acoustic phenomena: acoustic streaming[65] and acoustic radiation force acting on suspended objects in the path of wave propagation.[66] Either one of these phenomena or their combination has been used for droplet sorting. As a general feature of this approach, the size of the droplets and the physical (mechanical) properties of the liquids involved play a key role in the global performance of the methods using acoustic control, demanding at least a careful exploration of the working or optimum ranges of frequencies and geometrical designs to be used, for a given set of liquid properties and length scales of the suspended objects to be manipulated (*e.g.* droplets).

3.1 Surface acoustic wave (SAW) control

Surface acoustic wave (SAW) is a unique wave traveling on the surface of a piezoelectric substrate (such as lithium niobate, $LiNbO_3$). A SAW is typically generated by an interdigitated transducer (IDT) actuated with an AC electric field.[67] The IDT consisting of two comb-like electrodes is fabricated on a piezoelectric substrate. The dimensions of these microfabricated electrode fingers determine the resonance frequency, at which the oscillating displacement amplitudes of the substrate are maximized because the displacement generated by one finger-pair is reinforced by the neighbouring ones. The resonance frequency is expressed by $f = c/\lambda$, where λ is the substrate wavelength and c is the speed of sound in the substrate. In a conventional IDT design, the substrate wavelength λ is equal to the width of one finger-pair. A significant advantage of SAW for microfluidic manipulation is its operational frequency ranging from 10 to 1000 MHz, corresponding to wavelengths from approximately 4 to 400 μm, enabling the manipulation of particles and droplets with largely varying sizes. Microfluidic channels are typically placed in the path of the SAW propagation to couple acoustic energy into confined fluids for manipulation and sorting. Below, we will introduce two control methods with SAW, namely, traveling SAW (TSAW) control and standing SAW (SSAW) control.

3.1.1 Traveling surface acoustic wave (TSAW) control. A traveling surface acoustic wave, typically generated by a single set of IDTs, has been introduced to microfluidic devices for various applications including fluid mixing,[68,69] pumping,[70] particle separation[71–74] and enrichment.[75] The use of TSAW for microfluidic manipulation mainly relies on two acoustic phenomena, acoustic streaming and acoustic radiation. When the TSAW encounters any medium with a different speed of sound on top of the substrate and in the path of the wave propagation, the SAW partially radiates into the medium as a result of the mismatch in the speed of sound. The angle at which the SAW radiates along the interface is called the Rayleigh angle $\theta_R = \sin^{-1}(c_f/c_s)$, where c_f and c_s are the speed of sound in the fluid and in the substrate, respectively.[76] The absorption of acoustic wave through a fluid induces an acoustic body force along the propagation direction and can be expressed as[77]

$$F_B = \alpha c_f^{-1} I_{ac} e^{-2\alpha x} \tag{4}$$

where $\alpha^{-1} = \rho_f c_f^3/(b\omega^2)$ is the attenuation length in the fluid and I_{ac} is the initial acoustic intensity. Herein, ρ_f is the fluid density, ω is the angular frequency, and $b = 4/3\mu + \mu'$ is a function of the dynamic and bulk viscosities. The acoustic body force scales with ω^2 and thus results in time-averaged fluid flow that enables various streaming-based microfluidic manipulation techniques. A recent experimental study demonstrates that the magnitude of the streaming velocity also scales with ω^2 at a certain frequency range.[78] Because of this ω^2 scaling, high frequencies of more than 100 MHz are typically applied in microfluidic systems for effective streaming-based manipulation. The most recent study shows that the circulatory acoustic streaming generated by a highly focused 636 MHz TSAW field enables rapid capture of particles down to 300 nm.[75]

Suspended objects in the fluid (*e.g.* particles and droplets) with an acoustic impedance $Z = \rho c$ different from that of the fluid medium can scatter the TSAW. Due to the acoustic impedance mismatch along the interface, the transfer of momentum from the TSAW to the suspended object results in an acoustic radiation force on the scattering object. Experiments showed that this acoustic radiation force becomes dominant in an anisotropic scattering scenario that typically occurs when the particle size is small compared to the acoustic wavelength. Recent experimental studies found a critical value for polystyrene particles in water, *i.e.* $\kappa = \pi d/\lambda_f \geq 1$, where d is the particle diameter and λ_f is the fluid wavelength. Beyond this value, polystyrene particles can be effectively translated in a TSAW field.[71,72,79] For instance, a TSAW with a frequency higher than 100 MHz is required to effectively manipulate 6 μm polystyrene particles in water. Most recently, Collins *et al.*[74] demonstrated the separation of 1 and 2 μm polystyrene particles using the field of a 386 MHz TSAW. It is important to point out that the critical κ value for polystyrene particles experimentally determined in previous studies is not applicable to other suspended objects such as solid particles, cells and droplets. Since the TSAW field generally operates at high frequencies in microfluidic applications, acoustic streaming and acoustic radiation effects may coexist and require careful consideration.

For the application of TSAW in droplet sorting, Franke *et al.*[80] first demonstrated this concept in 2009 (Fig. 3a). The figure shows a PDMS microchannel with a Y junction placed on top of a $LiNbO_3$ piezoelectric substrate. The Y junction is designed with the upper branch having a lower flow resistance. All droplets flow into the upper branch because of its lower flow resistance, when the IDT is switched off. Once the IDT is excited at its resonance frequency of around 140 MHz, the piezoelectric effect generates a Rayleigh wave propagating toward the PDMS channel that is placed along the path of the wave propagation. The TSAW partially radiates into the channel and deflects the flow-through droplets along the wave propagating direction and in the experiment toward the lower channel. Although the authors attributed the droplet sorting mechanism to acoustic streaming, it is worth pointing out that the sorted droplets have a size of 20 μm, corresponding to $\kappa \approx 5.9$. Therefore, the radiation force on the droplets induced by the TSAW might also contribute to the droplet deflection. However, this hypothesis needs further theoretical and experimental verification. The team[81] later developed this concept further to a fluorescence-

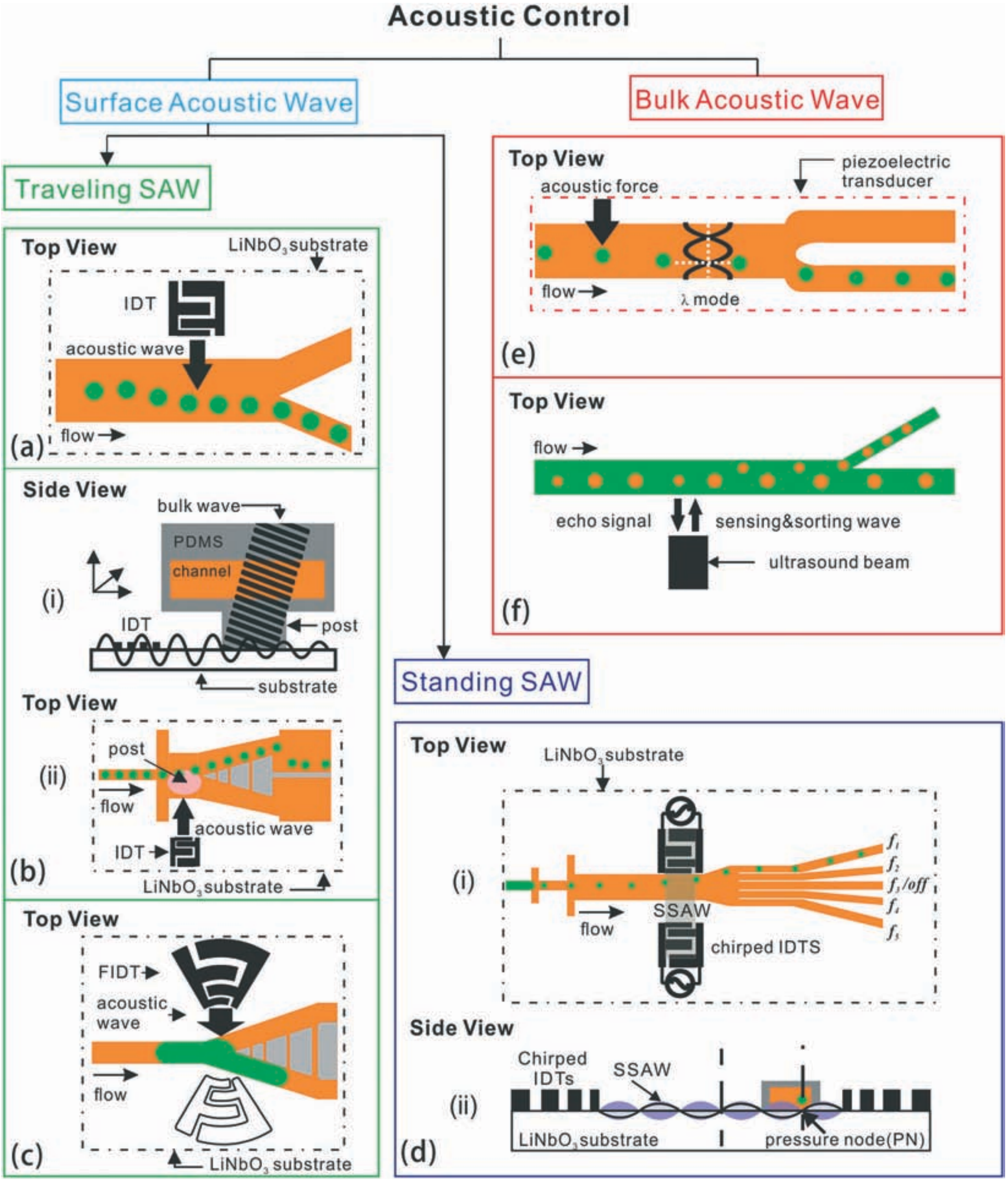

Fig. 3 Schematic sketch and classification of various acoustic droplet sorting principles. The orange parts represent oil flow and the green parts represent the aqueous flow. (a) A traveling surface acoustic wave (TSAW) is generated by an interdigitated transducer (IDT). When the IDT is activated, the TSAW deflects the droplets to the lower branch; (b) an acoustofluidic droplet sorter with a localized TSAW field. A PDMS post serves as a waveguide. (b-i) The TSAW propagates along the substrate surface and partially refracts into the PDMS at the post/substrate interface. A bulk wave is generated in the oil phase. (b-ii) The bulk wave introduced through the post region deflects the droplet to the upper channel; (c) droplet sorting using focused interdigital transducers (FIDTs). The blank IDT is unactuated. The liquid plug is steered at the Y junction by acoustic radiation and blocks the droplet movement to the upper channel; (d) droplet sorting using a standing surface acoustic wave (SSAW). (d-i) Two sets of IDTs are placed at two opposite sides of the channel and excited at the same frequency. The droplet is deflected by an acoustic radiation force generated in the SSAW field to the uppermost branch when the wave frequency is f_1. (d-ii) The location of the pressure node is controlled by altering the excitation frequency and the droplet is shifted to different pressure nodes; (e) droplet sorting using bulk acoustic wave (BAW) induced acoustophoresis. The droplet is attracted to the pressure nodal line and then moves to the lower branch; (f) droplets are detected and sorted by using a narrow ultrasound beam. Smaller droplets are pushed to the upper channel.

activated droplet sorting system (Fig. 3b). In this droplet sorting system, the confined fluid is not in direct contact with the substrate. Instead, the TSAW is guided into the fluid *via* a microstructured PDMS post sandwiched between the fluid and the substrate. The unique design enables localization of the acoustic field in the fluid above the PDMS posts, which are located in the main channel and approximately 200 μm upstream of the bifurcation. Similarly, a Y junction is used for sorting with the lower flow resistance branch for collecting the waste when the TSAW is switched off. Shunts connecting the two outlets are introduced in this sorting device to eliminate any possible pressure disturbances from the acoustic field. Fluorescent and non-fluorescent 20 μm aqueous droplets dispersed in a continuous fluorocarbon oil phase are introduced into the sorting region using a flow-focusing channel that ensures consistent fluorescence detection and sorting. An interrogation region collects the fluorescence signal from the droplets. Once the detected fluorescence intensity exceeds a threshold, a TSAW with a resonance frequency of 161 to 171 MHz is generated in an appropriate delay and travels along a narrow path to the post region.[79] When the TSAW reaches the post, the wave on the surface of the substrate partially refracts into the PDMS and propagates into a bulk wave with a Rayleigh angle of 21.8°. The bulk wave further propagates into the fluid and deflects the droplet through the post region to the upper channel side. The sorting speed is mainly limited by the minimum duration of the sorting pulse t_{pulse}, as only one single droplet can be present in the post region at once. The best sorting rate achieved was 3000 drops per second. Both numerical modelling and experimental observations have confirmed the substantial acoustic streaming in the post region with a localized acoustic field; however, the role of acoustic radiation force at $\kappa \approx 7$ in droplet sorting requires further investigations.

In a most recent study, Sesen *et al.*[76] made use of a TSAW for active steering of liquid plugs (Fig. 3c), which are defined as large droplets in contact with all four walls of a microchannel. Focused interdigitated transducers (FIDTs) are used in this study to generate a narrow TSAW field (λ = 60 μm and f = 64 MHz) in the two branches of a Y junction. A FIDT is fabricated using similar materials and techniques to those employed for a conventional IDT but consists of curved concentric electrodes. As the microscale plug enters the Y junction, a FIDT at one side is actuated for active steering. As the plug is large enough to generate an oil–water interface across the channel, the wave scattering at this interface due to the acoustic impedance mismatch results in a net acoustic radiation force along the interface. The acoustic radiation force basically generates an acoustic pressure at the neck of the bifurcation and blocks the same side branch, resulting in a larger volume of the plug being forced into the other side branch. Generally, a higher applied voltage, a smaller plug velocity and a smaller plug volume more likely lead to total steering. This TSAW-induced steering of microscale plugs mainly relies on acoustic radiation rather than acoustic streaming because of the use of a relatively low frequency.

The acoustic radiation force generated at the interface has also been used to translocate individual droplets in open environments[82,83] and for on-demand generation of water-in-oil droplets[84] and size control of droplet generation.[85] Therefore, both acoustic radiation and streaming effects induced by TSAW fields have been demonstrated for droplet sorting. To further explore the use of TSAW for droplet sorting, quantitative analysis of the radiation and streaming effects in different device settings is needed.

3.1.2 Standing surface acoustic wave (SSAW) control. The interference of two counter-propagating waves (waves from two different sources at the same resonance frequency or incident and reflected waves) can result in a standing acoustic field that forms a periodic spatial distribution of acoustic energy density. Assuming a spherical object is much smaller than the acoustic wavelength, the object, which is exposed to a standing acoustic field, is subjected to a time-averaged acoustic radiation force that can be described as[66]

$$F_r = -\left(\frac{\pi p_0^2 V_c \beta_f}{2\lambda}\right)\phi(\beta,\rho)\sin(2kx) \tag{5}$$

$$\Phi(\beta,\rho) = \frac{5\rho_c - 2\rho_f}{2\rho_c + \rho_f} - \frac{\beta_c}{\beta_f} \tag{6}$$

where p_0, λ, V_c, ρ_c, ρ_f, $\beta_c = (c_c^2\rho_c)^{-1}$ and $\beta_f = (c_f^2\rho_f)^{-1}$ are the acoustic pressure, acoustic wavelength, volume of the sphere, density of the sphere, density of the fluid, compressibility of the sphere, and compressibility of the fluid, respectively. These periodic spatial gradients of the standing acoustic field basically result in a periodic force field, leading to discrete pressure nodal and anti-nodal positions. Objects in a standing acoustic field preferentially migrate to the pressure nodal positions if the acoustic contrast factor $\phi(\beta,\rho)$ is positive and migrate to the pressure anti-nodal positions if $\phi(\beta,\rho)$ is negative. Unlike the continuous unidirectional translation solely limited by the wave attenuation in a traveling acoustic field, objects are trapped at discrete nodal or anti-nodal positions with a maximum translation up to one quarter of the wavelength in a standing acoustic field.

Typically, two IDTs are excited with the same AC signal to generate a one-dimensional (1D) standing SAW (SSAW) field in the region between the two IDTs. Microfluidic channels are placed on top of the SSAW field to couple the standing acoustic field into the fluids. The SSAW field accordingly manipulates objects flowing through the field *via* the acoustic radiation force, aligning these objects to the pressure nodal or anti-nodal positions. The application of SSAW fields in microfluidic devices has enabled various microscale manipulation techniques, including focusing,[72,86] switching,[87,88] patterning[89–91] and separation[92–96] of various microscale objects. For separation and sorting applications in particular, the wavelength is typically much larger than the object size to ensure a sufficient separation distance between dissimilar objects that is limited to 1/4 of the wavelength. This condition is also critical for the validity of eqn (5). As a result, a higher frequency can generate a larger radiation force. SSAW-based manipulation generally makes use of a relatively lower frequency compared to streaming-based manipulation. A device typically maintains one or two pressure nodal positions across the microfluidic channel, implying that the channel width is mostly smaller than one wavelength. The wave attenuation across one wavelength is too weak to create a substantial streaming effect, as the attenuation length along the water–$LiNbO_3$ interface is approximately 12.3× the substrate wavelength. Thus, the acoustic radiation force is the dominant effect in a majority of SSAW-based devices.

Similar to SSAW-based sorting of solid particles or biological cells, this manipulation technique has also been recently demonstrated for droplet sorting. Nam *et al.*[97] demonstrated the use of a SSAW field in sorting alginate droplets according to the number of cells encapsulated in the droplets. The sorting mechanism is based on the difference in overall density of droplets containing varying number of cells. Droplets with more cells experience larger radiation forces and thus migrate toward the pressure nodes at a higher rate, leading to density-based droplet sorting. This droplet sorting technique provides the possibility of collecting droplets containing a deterministic number of cells. Li *et al.*[98] further demonstrated multichannel droplet sorting using SSAW fields (Fig. 3d). In particular, two chirped IDTs with gradually increasing finger spacing (wavelength from 360 to 400 μm) are used in this study to allow tunability of the SSAW field. Water-in-oil droplets of 40 to 50 μm diameters moving through the SSAW field are pushed toward the pressure node by the acoustic radiation force. Tuning the frequency of the excitation signals applied on the two chirped IDTs can accordingly alter the position of the pressure nodes. As a result, droplets are sorted to multiple outlets at a rate of up to 222 drops per second. With integrated optical detection units, this droplet sorting technique has the potential to be further developed as a general droplet analysis platform.

3.2 Bulk acoustic wave (BAW) control

Unlike a surface acoustic wave which travels on the surface of a material, a bulk acoustic wave (BAW)[88,99,100] is an ultrasonic compressional wave that propagates in the bulk materials and is typically generated by bulk piezoelectric transducers instead of IDTs. A typical method of coupling BAWs into a microfluidic device is by constructing an acoustic resonator by affixing a bulk piezoelectric transducer underneath the channel. If the acoustic transducer is excited at resonance frequencies, $f_n^{\mathrm{res}} = c_f n/(2w)$ where w is the channel width and n = 1, 2, 3… refers to the first, second, and third harmonics, a standing acoustic field across the channel width can be generated (Fig. 3e). Materials with high acoustic impedance (*e.g.* silicon and glass) are generally used to construct the BAW-based microfluidic devices, because the huge difference in acoustic impedance at the fluid/structure interface can reflect the major acoustic energy back to the fluid to create a strong standing wave field. Separation of solid particles and biological cells using BAWs in microfluidic devices has been successfully demonstrated in various previous studies.[101]

As early as 2005, Petersson *et al.*[102] successfully applied a bulk standing acoustic field to separate lipid droplets from blood. Efficient separation of lipid droplets and blood cells relies mainly on the opposite acoustic contrast factor of the two types of objects. Basically, lipid droplets and blood cells in aqueous solutions move to the pressure anti-nodal and nodal positions, respectively. Leibacher *et al.*[103] recently further demonstrated versatile droplet manipulation techniques including droplet fusion, sorting and medium exchange using BAW-based standing fields (Fig. 3e). The microchannels were fabricated in silicon wafers using an inductively coupled plasma (ICP) etching system. Deionized water and silicon oil were used as the dispersed phase and the continuous phase, respectively. The water-in-oil droplets have a positive acoustic contrast factor and thus tend to migrate toward the pressure nodes. In the droplet sorting study, the excitation frequency at 463 kHz and 979 kHz enables switching between the λ mode and the $\lambda/2$ mode such that the nodal position is shifted between the upper and lower outlets for sorting. In contrast to SAW-based devices, BAW-based devices are operated at a relatively lower frequency (0.1–10 MHz), which allows the manipulation of larger droplets up to 500 μm because of the use of a longer wavelength.

Lee *et al.*[104] introduced a 30 MHz ultrasound beam to sort 100 μm lipid droplets in water (Fig. 3f). Different from previously discussed BAW-based microfluidic systems with silicon channels, a PDMS channel with a bifurcation was used for droplet sorting in this study. The 30 MHz ultrasound beam was generated using a lithium niobate single element transducer that is placed outside the channel with the axis perpendicular to the channel wall. The acoustic impedance of PDMS and water is similar, leading to a minimum sound reflection at the PDMS–water interface. Therefore, the acoustic transducer and the microfluidic device are both immersed in a water bath to maximize the ultrasonic transmission into the microfluidic channel. A single cycle of a 30 MHz sinusoidal wave was applied on the acoustic transducer to generate pulsed waves for sensing flow-through lipid droplets in water. Droplets with different sizes return different echo signals that are received by the same transducer. An integrated backscatter (IB) coefficient[105] was used to evaluate and differentiate the differently sized droplets. When the IB coefficient of a 100 μm droplet is detected, a burst of 2000-cycled 30 MHz sinusoidal signals subsequently created an acoustic radiation force, pushing the target droplet to the collecting branch. Relatively high sorting efficiencies of 99.3% and 85.3% for 50 μm and 10 μm lipid droplets, respectively, have been obtained using this method. Although the authors did not clearly explain whether this radiation force rises from a traveling wave or a standing wave, the radiation force seems to come predominantly from the traveling wave, since the wave reflection at the PDMS–water interface is very limited. Also, the 100 μm lipid droplets in a 30 MHz traveling wave corresponds to $\kappa \approx 6.3$, indicating that the traveling wave is very likely to generate a substantial radiation force on suspended lipid droplets in water for sorting.

4 Magnetic control

The manipulation of droplets *via* a magnetic field has numerous applications in both chemical and biological studies.[106–109] The main advantage of magnetic control is the ability to employ wireless control of droplets containing biological reagents and chemical samples. In terms of fabrication and integration, magnetic manipulation is relatively easy to implement. However, the fundamental drawback is the need for magnetic materials in the fluidic system, which sometimes could be problematic for chemical/biological compatibility. In terms of droplet sorting, ferrofluid[110] and magnetic beads[111] are often used. The exerted magnetic field affects droplets through the interaction with these magnetic materials. Another drawback of magnetic sorting is the slower response compared to other methods. The switching frequency is often on the order of several Hertz or lower.

Magnetic manipulation of droplets can be classified based on the type of magnet used. The approaches discussed here make use of either an electromagnet or a permanent magnet. An electromagnet provides an on-demand magnetic field with field strength tunable with the applied current. However, electromagnets could produce excessive heat at high currents. The induced heating may be detrimental to heat-sensitive biological reactions, such as PCR,[112] and most biological samples.[113] In light of these limitations, permanent magnets[114] are often preferred over electromagnets in microfluidic platforms. Permanent magnets are often placed at the side of the device to provide magnetic actuation. The magnetic field strength is adjustable by changing the distance between the magnets and droplets.

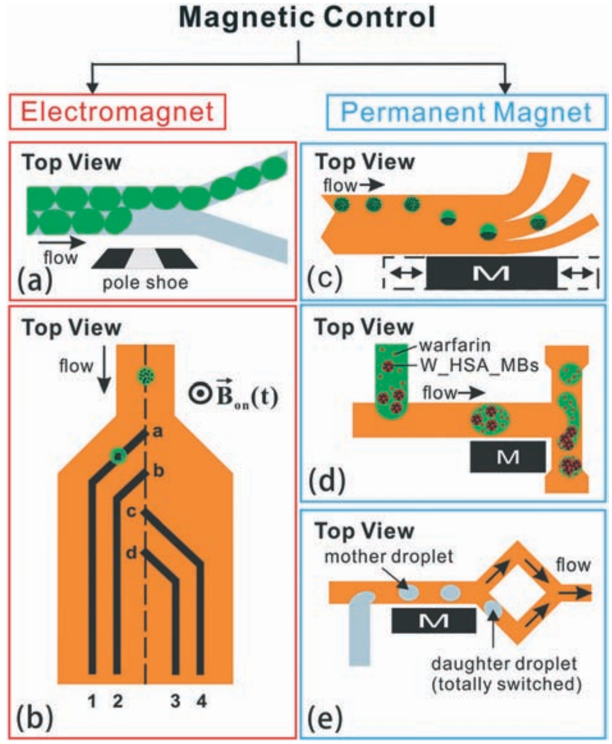

Fig. 4 Schematic sketch and classification of droplet sorting with a magnetic field. The orange parts represent oil flow and the green parts represent the aqueous flow. (a) The fluid in blue is oil-based ferrofluid. A pointed pole shoe (electromagnet) adjacent to the main channel generates an inhomogeneous magnetic field. The ferrofluid flows to the lower branch and forms a ferrofluidic induced "valve". Droplets are then sorted to the upper branch; (b) magnetic rails in black are placed under the main channel. A single droplet with magnetic beads is directed by the magnetic field to rail 1 when the droplet reaches point a; (c) magnetic beads inside the droplets are attracted by the magnet and causes the droplets to deflect vertically. The magnet can be placed along the channel direction and has three different states, namely, left, middle and right, which result in droplet deflection into the top, middle and lower branches, respectively; (d) warfarin–HSA (human serum albumin) binding is immobilized on the surface of the magnetic beads (W_HSA_MB). Small red points represent dissociative warfarin molecules and black points represent HSA bound magnetic beads. Each droplet is split into two equal volume daughter droplets with the lower one having a higher concentration due to the attraction of the magnet; (e) the dispersed phase in blue is water-based ferrofluid. A permanent magnet is placed at the lower side of the channel to attract and sort droplets.

4.1 Electromagnet

In 2009, Surenjav *et al.*[115] introduced droplet sorting by coupling an electromagnet with a microfluidic platform (Fig. 4a). In the proposed method, ferrofluid[116–118] was used as the continuous phase rather than the dispersed phase[119] to provide magnetic sorting. Developed by NASA in 1963, ferrofluid is a colloidal fluid with superparamagnetic properties[120] due to the presence of magnetic nanoparticles. These nanoparticles have a typical diameter of about 10 nm and are well dispersed and separated by a proprietary surfactant. The surfactant stabilizes the nanoparticles and prevents agglomeration.

Deionized water is used as the dispersed phase fluid to generate a gel emulsion in the method. The water-in-ferrofluid system can be generated by either step-emulsification[121] or cross-shear in a T-junction.[122,123] The gel emulsion produced is stable and no additional surfactant is required. As the gel emulsion moves into a microchamber, the droplets are arranged into certain patterns depending on the flow conditions and the geometry of the channel. The "bamboo" (drops in one row) and "zigzag" (drops in two rows) structures are commonly formed. When the gel emulsion flows to a bifurcation, droplets are either split (for the bamboo structure) or separated into two subchannels (for the zigzag structure) based on the upstream arrangement. In order to realize droplet sorting, an inhomogeneous magnetic field is applied by placing the pole shoe of the electromagnet close to the channel. The inhomogeneous magnetic field[124,125] causes the ferrofluid to flow toward the region with a larger magnetic field strength and results in the formation of a ferrofluid plug at the lower branch, thus creating a stop valve there and sorting the droplets to the upper channel.

In 2015, Teste *et al.*[126] proposed a magnetic rail to guide and sort droplets with the integration of an electromagnet (Fig. 4b). Four magnetic rails are made of PDMS mixed with ferromagnetic iron particles. The composite mixture are then integrated under the main flow channel. A homogeneous magnetic field is generated at the centre of an electromagnetic coil perpendicular to the device plane. Droplets are generated by sequentially aspirating both the aqueous suspension of magnetic beads and the oil phase. The droplets then enter the device one at a time to avoid interference. A weak magnetic field has less effect on the magnetic beads inside the droplets. However, near the rails the magnetic field gradient would sharply increase, attracting the droplets containing magnetic beads to the rails. The sum of the force on the droplet near the rail in the horizontal direction is given by:

$$\vec{F}_{\mathrm{l}} = \vec{F}_{\mathrm{m}} + \vec{F}_{\mathrm{d}} = \left(F_{\mathrm{d}}\cos\theta\right)\vec{e}_x + \left(F_{\mathrm{m}} - F_{\mathrm{d}}\sin\theta\right)\vec{e}_y \tag{7}$$

where F_{m} is the magnetic force, $F_{\mathrm{d}} = 6\pi\eta r\Delta v$ is the drag force from the oil flow, and θ is the angle between the rail and the flow direction of the oil. The resulting force from magnetism and oil flow drives the droplets along the rail. Thus, droplets could be sorted with different tracks by actuating the electromagnetic field.

4.2 Permanent magnet

Zhang *et al.*[127] introduced magnetic sorting using a permanent magnet and superparamagnetic magnetite (Fe_3O_4) nanoparticles (Fig. 4c). Water droplets with well dispersed particles are immersed in the oil phase (silicon oil or fluorocarbon oil). The two phases are then injected into the microchannels. Three outlets are placed downstream with varying flow resistances ($R_1 < R_2 < R_3$). In the absence of a magnetic field, droplets spontaneously enter the top channel with a lower flow resistance. By placing the permanent magnet close to the lower channel, the nanoparticles are magnetized but will not be dragged out of the droplets due to the relatively low magnetic field gradient. Droplets under the influence of the magnetic force are deflected to the lower channel countering the Stokes' drag,[128] which is in the opposite direction. The deflection distance corresponds to the lateral length of the deflecting region and the magnet can be moved along the channel direction to vary the magnetic field strength. Three different states are set for the magnet position, *i.e.* left, middle and right with respect to the bifurcation and referred to as full, half and zero deflection. In these three cases, deflected droplets enter the lower, middle and upper channels, respectively. A relatively higher efficiency can be obtained with this sorting method for various nanoparticle concentrations, flow rates and droplet sizes. In general, a sorting rate of about 10 drops per second can be achieved.

Since magnetic beads are highly compatible with many biomolecules,[129] they can therefore be used as an efficient carrier.[130] In 2011, Lombardi *et al.*[7] performed microfluidic droplet-based screening by employing protein–bead binding (Fig. 4d). First, human serum albumins (HSAs) are immobilized on the surface of the magnetic beads (MBs) to form the first binding (HSA_MBs).[131] This coupling procedure is carried out in a special buffer. Second, the beads are incubated with warfarin solution to carry out the drug–protein binding until chemical equilibrium is achieved. Then, the aliquot of warfarin and bead suspension is injected into the microchannel. The droplets are generated at a T-junction by shearing from the oil flow. Another T-shaped channel with two thinner branches is patterned to split the initial droplet into two equal sized daughter droplets downstream. Most of the magnetic beads are attracted to the magnet placed at the corner of the T-channel. Since the warfarins and proteins are bound onto the magnetic beads, a daughter droplet with a high concentration of warfarin–HAS can be isolated.

In 2016, Li *et al.*[132] introduced another method for the manipulation of ferrofluid droplets using a permanent magnet (Fig. 4e). Ferrofluid is used as the dispersed phase. The group demonstrated the controlled breakup of ferrofluid droplets and, under special conditions, sorting of the droplets. Water-based ferrofluid droplets are generated by the shearing oil flow at a T-junction and directed to a bifurcation for splitting or sorting. When the mother droplet enters the Y-shaped junction, the inhomogeneous magnetic field attracts more volume of the ferrofluid to the lower branch, inducing an asymmetric breakup. In essence, the volume ratio of the lower daughter droplet to the upper daughter droplet ($V_{\mathrm{l}}/V_{\mathrm{u}}$) increases as the flow rate ratio of the dispersed phase to the continuous phase ($Q_{\mathrm{d}}/Q_{\mathrm{c}}$) decreases and the magnetic flux density increases. A special flow pattern was observed with non-breakup emerging and all mother droplets flow to the lower channel. Based on this behaviour, sorting of bigger droplets and full sorting could be performed.

5 Pneumatic control

Droplet sorting by pneumatic control resorts mainly to the variation of hydrodynamic pressure through the deformation of the microchannel. These variations can be induced by incorporating mechanical elements into the system in response to control inputs. To this end, external pressure or actuated microvalves are used to adjust the hydrodynamic resistance in the carrier flow. The energy budget needed to achieve droplet sorting as well as the system durability determines its quality and performance. In general, the energy efficiency of these methods is quite low, the device lifetime is poor, and the response time/throughput is modest, while offering a virtual independence of the liquid properties and droplet sizes.

5.1 Hydrodynamic pressure

Wu *et al.*[133] introduced a droplet sorting mechanism by applying a depression to different subchannels of the system (Fig. 5a). The sketch shows an example of a cross-shaped channel patterned to sort droplets encapsulating a single cell. The sorting mechanism relies on an additional oil flow introduced through source 2 (S_2). Outlet 1 (O_1) and outlet 2 (O_2) are connected to a negative pressure system. Droplets are generated at a flow-focusing channel with encapsulated cells due to the depression at O_1 and O_2. Photomultipliers (PMT) and other optical sensing devices are used for detecting the content of cells in the droplet. While a constant depression is applied on O_2, the pressure connected to O_1 can be switched between higher and lower states. Initially, the pressure ratio between O_2 and O_1 is set to be 0.75, which forms a hydrodynamic gating valve.[134–136] Most of the fluid from source 1 (S_1) enters channel O_1 and the incoming flow from source 2 (S_2) enters channel O_2. Each droplet is detected before reaching the cross channel. Once the droplet with a single cell is detected, the signal will be sent to the control system, and the pressure on O_1 will be switched to a higher state after a certain delay. The pressure balance at the cross channel is then altered and the hydrodynamic gate opens allowing the target droplet to pass. Both O_1 and S_2 are in a "holding" state until the pressure state on O_1 is switched back. With less outside impact and additive requirement, this device has good biocompatibility in applications. Wu *et al.* achieved a typical single-cell encapsulation rate of 94.1% with Hela cells.

Exploiting an external pressure source, Cao *et al.*[137] developed a fluorescence-activated microfluidic droplet sorter with the simple deflection mechanism of pushing the target droplet to a side channel by an oil flow pulse (Fig. 5b). To generate droplets, an aqueous particle suspension is sheared by fluorocarbon oil flow.[138] The water-in-oil flow enters the downstream straight waste channel without any interference, due to the hydrodynamic resistance difference between the two outlets. An actuation channel is connected at the junction of the collection channel. The actuation is performed with compressed air and controlled by a solenoid valve. The sorting mechanism is achieved by a first step of interrogation of the content inside the droplet by laser-induced fluorescence (LIF) before the junction. The PMT transmits the fluorescence signal containing information on the number of the fluorescent beads or cells inside the target droplet to a comparator. Droplets naturally flow into the waste channel due to the asymmetric design of the bifurcation.[139] When the optical signal reaches a predefined level,[140] the droplet is identified as a target. An input signal is sent to the microcontroller and then to the solenoid valve after a delay. A quick open–close action of the valve causes a pressure pulse flow in the oil at the actuation channel, which is transmitted to the junction and eventually directs the droplet to the collection channel. This setup can achieve a sorting rate of at least 30 drops per second. However, the accuracy deteriorates as the sorting rate increases. In the case of droplets containing beads, an accuracy of 97% at a rate of 5 drops per second decreases to 90% at a rate of 30 drops per second. Similar designs were introduced by Aubry *et al.*[141] with two side channels and by Shemesh *et al.*[142] with pulse flow generated by a piezoelectric actuated membrane. Zhang *et al.*[143] also induced a suction force from a capillary-tuned solenoid microvalve to actively sort droplets.

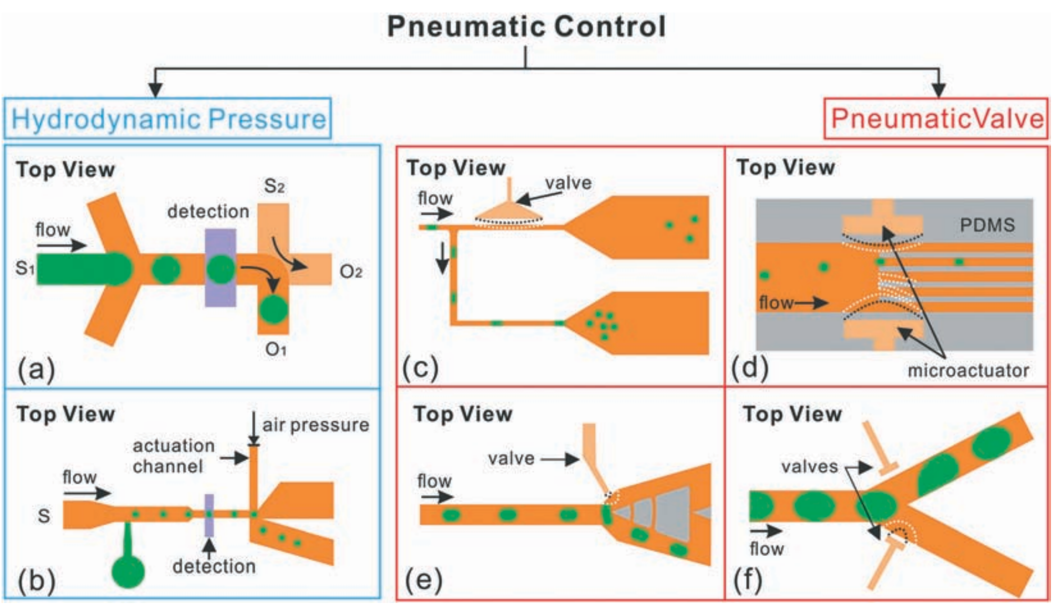

Fig. 5 Schematic sketch and classification of droplet sorting with pneumatic control. The orange parts represent oil flow and the green parts represent aqueous flow. The deformation of valves and that of channels are represented by black and white dotted lines, respectively. (a) Hydrodynamic gating occurs by connecting outlet 1 (O_1) and outlet 2 (O_2) to a negative pressure system. The pressure ratio of O_2/O_1 is tunable. When the value is 0.75, droplets move to O_1; (b) the actuation channel is connected to compressed air and controlled by a solenoid valve. Target droplets are sorted to the lower collection channel when the air pressure is increased; (c) a single-layer valve is at one branch of the sorter with a flexible elastomeric membrane separating two microchannels. Droplets are deflected to the lower branch when the valve is actuated; (d) four parallel walls separate the main channel into five sampling channels and two microactuators are patterned at two sides. When the microactuators are actuated, walls will be bent under the condition that only one sampling channel remains fully open. Droplets then flow into the sampling channel. The selection for the sampling channel is by altering the pressure in the two microactuators; (e) a single-layer membrane valve consists of an air channel abutting one side of the bifurcation. Droplets flow to the lower channel when the valve is actuated; (f) PDMS walls deformed by pneumatic pressures. When the bottom valve is actuated, droplets flow to the top branch.

5.2 Pneumatic valve

Valves are widely used in microfluidics[144–150] to perform different complex applications. The valves rely on the elasticity of the materials to perform the rectification action. The sorting process is achieved by deforming the microchannel walls. As the flow pattern of the continuous phase is changed, the trajectories of droplets are correspondingly changed.[151]

Abate *et al.*[152] proposed a microfluidic device for droplet sorting based on membrane valves in 2008 (Fig. 5c). In contrast to other multi-layer valves used previously,[153–157] the single-layer design is much simpler in fabrication. The inherent elasticity of PDMS is essential to the sorting action. Fig. 6c shows that the valve channel is made of a long hollow strip patterned in parallel to one branch of the T junction and separated by a thin elastomeric PMDS membrane. This valve is actuated by varying the pressure on the hollow strip to deform the membrane. When the valve is not actuated, all droplets go into the upper waste channel because of its lower fluidic resistance. When the valve is actuated, the valve channel is obstructed by the adjacent pressurized hollow strip, and the droplets are steered to the lower branch spontaneously. Interestingly, a recent work by Chen *et al.*[158] used the suction effect by relaxing valves and obtained a similar result.

The use of the elasticity of PDMS for sorting purposes is further developed by Yoon *et al.*[159] Fig. 5d shows a multichannel structure designed for additional classification features of the droplets. The adequate formulation of resin and curing agent yields a highly elastic PDMS that is used to form a brush of five nearly parallel sub-channels coming from the main one. The five channels are separated by thin walls. Two microactuators are placed side by side in the flow channel at the inlets of the subchannels. All subchannels have the same width of 40 μm. Droplets enter this structure one by one from a collective drain channel through squeezing. Pneumatic pressure differences up to 250 kPa are applied on the two actuators to deform the channel and parallel walls. Depending on the combination of the applied pressures, five possible configurations can be obtained to allow each individual channel to be unobstructed. A domino-like deformation of the parallel walls is observed in these processes to sort droplets. However, the required large deformation of the channel walls eventually affects the device durability, causing inaccuracies or even channel damage. In addition, the speed of the one-by-one droplet sorting is severely limited.

Fig. 5e shows another device reported by Abate *et al.*[160] A thin, finger-like valve is patterned at one side of the bifurcation. Its tip "touches" the bifurcation at the Y junction. Shunt structures are used to balance the downstream resistance to avoid possible interference. A slight asymmetry of the bifurcation is originally designed so that droplets flow through the upper waste branch when the valve is not active. To collect the target droplets, fluorescence detection is applied before droplets reach the bifurcation. When a target droplet approaches the Y junction, a slight increase in pressure inside the valve is observed, squeezing the upper branch of the junction and forcing the droplet to flow into the lower branch. Conceptually, this method is analogous to the one depicted in Fig. 5c. However, accurate sorting with errors below 0.01% can be achieved, since the channel width at the junction is narrow and the deformation area is closer to the droplets. Also, the slight change in pressure induced by the valve extends the device durability induced by the deformation.

Furthermore, Yoon *et al.*[161] presented an active and precise method to control droplets at the Y junction with two pneumatic valves. The valves are placed close to the

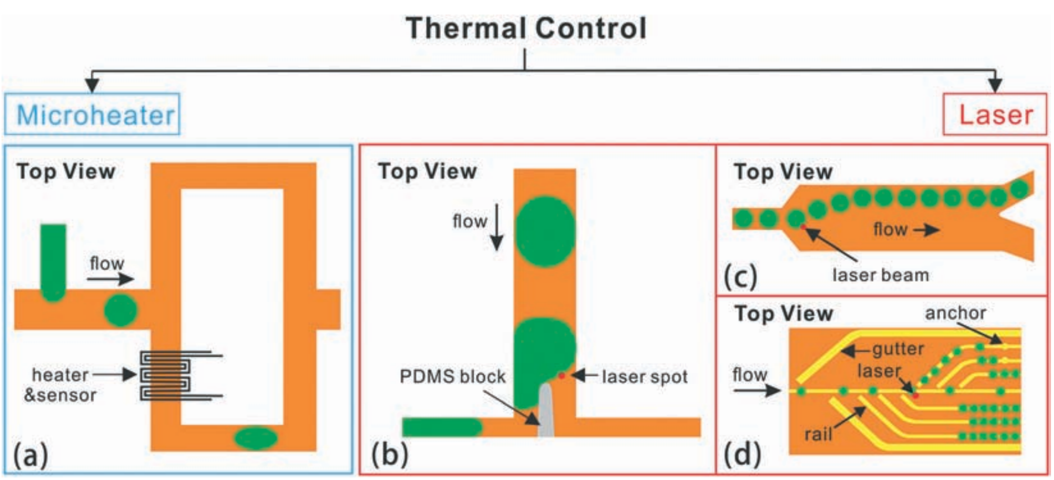

Fig. 6 Schematics and classification of droplet sorting with thermal control. The orange parts represent oil flow and the green parts represent aqueous flow. (a) A microheater reduces the flow resistance on the lower branch and droplets are sorted to the lower branch; (b) a laser spot induced a thermocapillary effect that squeezed the droplet to the left branch; (c) laser induced sorting at high speed. When the laser is activated, droplets flow to the top branch; (d) laser induced droplet sorting combined with storage rails and anchors. Droplets flow to the rail when the laser is actuated.

bifurcation point (Fig. 5f). The flexibility in the adjustment of hydraulic resistance of the channels allows not only droplet sorting but also droplet division with different volume ratios. Various channel sizes were investigated in their study. The team concluded that using narrower channels and keeping the same valve size allowed for a wider range of volume ratios of droplet division. Specifically, for a main channel width of 100 μm with both sub-channel widths of 50 μm when pressures of 0 and 250 kPa were applied on the lower and upper actuators, respectively, droplets went entirely into the channel with a lower resistance. This configuration can be used for sorting purposes. Owing to the smaller width of the channel, the required deformation for sorting is kept to a minimum, reducing the potential for device damage. The sorting accuracy increases with narrower channels. A working rate of 1 Hz was achieved with this concept.

6 Thermal control

Droplet sorting with thermal control exploits the advantages of the thermocapillary effect[162–164] on the microscale. Both resistive heating and focused laser beam are generally utilized to generate thermocapillary forces. In resistive heating, the microheater and temperature sensor require precise alignment at a specific location.[165,166] On the other hand, the use of a laser beam offers the flexibility to drive droplets to different locations of interest. Resistive heating can be coupled with additional resistive elements to provide *in situ* localized temperature readings. This feature is extremely useful for temperature sensitive biological processes such as PCR.[167] Using the laser beam, an off-site temperature measurement is often required to calibrate the temperature at different power beam intensities. These methods are generally restricted to specific applications where all other general alternative approaches so far discussed fail to fulfil the key demands of the systems involved.

6.1 Resistive heating

Yap *et al.*[168] first introduced a thermally mediated control of droplets with the use of an integrated microheater and a temperature sensor in 2009 (Fig. 6a). A T-junction bifurcation channel is used for both droplet sorting and size manipulation. Water-in-oil droplets are first generated by shear forces. The mother droplet moves downstream and breaks into two daughter droplets at the bifurcation. The compression and stretching from the oil flow[169,170] split the droplet evenly due to the axisymmetry of the bifurcation. In order to manipulate the droplets, a microheater and a temperature sensor are placed at one side of the bifurcation. Volumetric flow rates are carefully controlled so that the droplets enter the sorting loop one at a time. An activated microheater creates an asymmetric temperature field resulting in different fluidic resistances in the two branches. A high temperature gradient is also generated at the lower channel. Different from the thermomechanical case,[171] resistive heating decreases the viscosity of the oil, which in turn reduces the fluidic resistance and interfacial tension to the water phase.[172,173] As a result, the mother droplet breaks up and a larger portion of it is drawn into the lower branch, which creates daughter droplets of different sizes. If the temperature is greater than 36 °C, sorting is achieved as the mother droplet moves into the heated branch.

6.2 Laser heating

Lasers are commonly used in lab-on-a-chip modules for optical sensing and thermal manipulation.[174,175] In droplet sorting, laser beams are focused near the interface of the water and oil phases to generate thermocapillary stresses.[176] This stress has a direction originating from the focal point of the laser and causes the droplets to deflect away. Various channel structures can also be coupled to implement different sorting purposes.

Baroud *et al.*[177] proposed for the first time the use of lasers for droplet sorting in 2007 (Fig. 6b). The group observed that the interface between water and oil could be effectively blocked, when the laser beam is turned on. Interestingly, the study shows that the interfacial tension increases with temperature. They postulated that the increase in interfacial tension is caused by the migration of the surfactants and the thermocapillary effect.[178–180] The thermocapillary force[181] can be described as

$$F = -2\sqrt{\pi}\,\frac{\mu_2}{\mu_1+\mu_2}\Delta T \gamma' \frac{hw}{R} \qquad (8)$$

where μ_1 and μ_2 are the dynamic viscosities of water and oil, respectively, ΔT is the maximum temperature difference between the hot spot and the ambient environment, $\gamma' = \partial\gamma/\partial T$ is the rate of change of surface tension with temperature, R is the local radius of curvature of the droplet, h and w are the typical scales for velocity variations in the radial and azimuthal directions.

Fig. 6b shows a symmetric bifurcation configuration. When the laser is turned off, the droplet will be split by the notch into two equal daughter droplets entering different branches. The laser spot applied on the right will block the droplet. As a result, the droplet moves to the left. This thermally induced valve can be positioned at a different location to sort droplets to the desired branch.

Robert de Saint Vincent *et al.*[182] performed a similar study by injecting droplets into a chamber with two asymmetric outlets. A laser beam is used to deflect the droplets at the main chamber (Fig. 6c). The rate of change of the interfacial tension with temperature ($\partial\gamma/\partial T$) is greater than zero. This result is similar to the case reported by Baroud *et al.*[177] The generated thermocapillary force pushes the droplet to the upper outlet. The thermally induced deflection is affected by several factors. In general, the flow velocity, droplet radius and optical absorption could influence the deflection rate and deflection force acting on the droplets.[177,183–185]

Rails and anchors can be combined and integrated for laser induced sorting. This concept was introduced by Fradet *et al.*[186] in 2011 (Fig. 6d). The application of rails and anchors in droplet sorting was demonstrated in other previous works.[15,16,187] However, in contrast to passive sorting by droplet size, laser induced sorting could be achieved on-demand. Droplets entering a chamber are first guided by a central rail. Paralleled storage rails with anchors in the form of square grooves are patterned by sides of the main rail with approaching parts to the main channel. A laser beam is focused on the surface of the droplet and deflects the droplet to the storage rail by the induced thermocapillary force. Thus, the droplet is subsequently guided by the storage rails.

7 Conclusion and perspective

The present review summarizes recent advances in droplet sorting. A variety of different active sorting concepts have been reported. We categorised and discussed the different concepts according to electric, acoustic, magnetic, pneumatic and thermal actuation schemes. In Fig. 7, we consider six general performance categories: (i) response time and throughput, (ii) ease of fabrication, (iii) the cost of the experimental setup, (iv) accuracy and selectivity, (v) device lifetime, and (vi) dependence on the droplet size. According to these performances, the five actuation concepts are quantified and discussed below.

Electric actuation appears to be the most robust and has the highest sorting rates/response times reported. These attributes, together with high accuracy and selectivity, result in the highest general score (having the largest area in Fig. 7). One main disadvantage of electric actuation is the relatively higher experimental setup cost as compared to other active actuation schemes. Often, a waveform generator and a voltage amplifier are required to produce the required electric field. Acoustic actuation relies on both acoustic streaming and radiation force to manipulate droplets, with high inherent limitations (thus resulting in the lowest overall score among the methods discussed), but once carefully designed and tuned, the devices using these methods offer high durability and good selectivity and accuracy. On the other hand, acoustic actuation imparts high energy into the fluidic systems. This may result in unwarranted heating which may not be suitable for some applications. Magnetic actuation often provides a lower sorting rate and requires the use of magnetic materials, which entail a high generic barrier for most applications; however, their relatively simple fabrication steps and low cost make them attractive for specific applications. Pneumatic sorting always entails mechanical deformation of either the channels or intermediate walls, wells or separators by active valves, which affects the device durability. Besides, the mechanical nature of these methods yields low response time and throughput. In contrast, they generally offer the highest degrees of freedom for chemical formulation, geometries, length scales and droplet size. Thermal actuation has limited biological applications due to the heat sensitivity of the items involved. However, these methods generally offer significant accuracy, sensitivity, and response time when all other methods fail to fulfil the specific demands of certain applications.

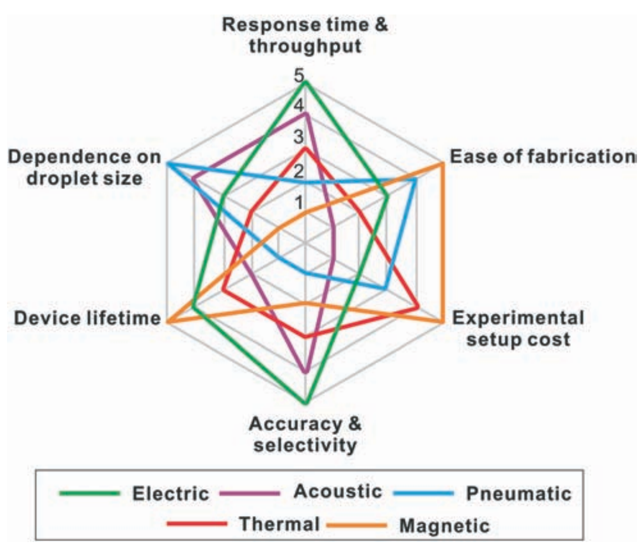

Fig. 7 Schematic sketch to compare between different active methods of droplet sorting. Six performance categories are used for comparison: (i) response time and throughput, (ii) ease of fabrication, (iii) cost of the experimental setup, (iv) accuracy and selectivity, (v) device lifetime, and (vi) dependence on the droplet size. A scale of 1 to 5 is used to rank each category where 5 represents the highest score.

State-of-the-art droplet-based microfluidics technology deals with a massive number of droplets. Currently, droplets are generated, manipulated and detected without the ability to track and monitor them. Our vision for the future of this technology is finding a way to address or encode droplets or droplet trains. All manipulation tasks should be based on the information available through these encoding schemes. We envision that either individual droplets or a droplet train should be tagged and coded with information. Coding mechanisms could be optical or magnetic. Coding and decoding could be carried out wirelessly through devices integrated into the microfluidic device. A droplet packet or train could be coded similarly to a serial bit stream in digital electronics. Some droplets on the train could have a basic prescribed function such as start droplet, stop droplet, information storage droplet and error check droplet, as it is well established in informatics. Thus, manipulation tasks are subsequently performed on the same train based on the information available. In this regard, active droplet sorting should be deemed a basic key process in any complex, active microfluidic system design.

If droplets or droplet trains are addressable as envisioned above, the next possible advance is digital processing of these droplets in the same manner as that made with dual electric states in the form of bits and bytes in information technology. Instead of designing customized and *ad hoc* systems as described in this review, more generic microfluidic devices and vitally necessary building blocks can be developed to process the addressable droplets such as shift register, flip-flop, serial-to-parallel and parallel-to-serial converters. Combining these digital microfluidic devices would allow for functional, complex, generic, flexible and powerful systems, covering specific technological areas and applications where electronics alone cannot compete or cannot offer an integrated chemical or biochemical functionality. The most powerful aspect of this concept is perhaps the compatibility with digital electronics that allows for programmability and storage of droplets and droplet trains.

Acknowledgements

S. H. Tan and N. T. Nguyen gratefully acknowledge the support through the Griffith University Post-doctoral fellowship, New Researcher grant, linkage grant (LP150100153), Discovery grant (DP170100277), DECRA fellowship (DE170100600) and Griffith University–Peking University collaboration grant. H. D. Xi, H. Zheng and W. Guo gratefully acknowledge the support from the National Natural Science Foundation of China (through grant no. 11472094), the Fundamental Research Funds for the Central Universities of China, the Peacock Plan of Shenzhen Municipal Government (through contract no. KQCX20130627094615415) and the Fundamental Research Fund of Shenzhen Municipal Government (JCYJ20140417172417119). Y. Ai gratefully acknowledges the support from the Singapore Ministry of Education Academic Research Fund Tier 2 (T2MOE1603). Y. Huang gratefully acknowledges the support through the Griffith University–Peking University collaboration grant.

References

1 M. U. Kopp, A. J. De Mello and A. Manz, *Science*, 1998, **280**, 1046.
2 N. Pamme, *Lab Chip*, 2007, **7**, 1644.
3 Z. Z. Chong, S. H. Tan, A. M. Gañán-Calvo, S. B. Tor, N. H. Loh and N.-T. Nguyen, *Lab Chip*, 2016, **16**, 35.
4 I. Barbulovic-Nad, H. Yang, P. S. Park and A. R. Wheeler, *Lab Chip*, 2008, **8**, 519.
5 K. Choi, A. H. Ng, R. Fobel and A. R. Wheeler, *Annu. Rev. Anal. Chem.*, 2012, **5**, 413.
6 J. C. Baret, O. J. Miller, V. Taly, M. Ryckelynck, A. El-Harrak, L. Frenz, C. Rick, M. L. Samuels, J. B. Hutchison, J. J. Agresti, D. R. Link, D. A. Weitz and A. D. Griffiths, *Lab Chip*, 2009, **9**, 1850.
7 D. Lombardi and P. S. Dittrich, *Anal. Bioanal. Chem.*, 2011, **399**, 347.
8 S.-Y. Teh, R. Lin, L.-H. Hung and A. P. Lee, *Lab Chip*, 2008, **8**, 198.
9 E. Kadivar, S. Herminghaus and M. Brinkmann, *J. Phys.: Condens. Matter*, 2013, **25**, 285102.
10 Y.-C. Tan, Y. L. Ho and A. P. Lee, *Microfluid. Nanofluid.*, 2008, **4**, 343.
11 A. C. Hatch, A. Patel, N. R. Beer and A. P. Lee, *Lab Chip*, 2013, **13**, 1308.
12 H. Maenaka, M. Yamada, M. Yasuda and M. Seki, *Langmuir*, 2008, **24**, 4405.
13 Y.-C. Tan, J. S. Fisher, A. I. Lee, V. Cristini and A. P. Lee, *Lab Chip*, 2004, **4**, 292.
14 H. N. Joensson, M. Uhlén and H. A. Svahn, *Lab Chip*, 2011, **11**, 1305.
15 D. HyunáYoon, *RSC Adv.*, 2014, **4**, 37721.
16 P. Abbyad, R. Dangla, A. Alexandrou and C. N. Baroud, *Lab Chip*, 2011, **11**, 813.
17 D. R. Link, E. Grasland-Mongrain, A. Duri, F. Sarrazin, Z. Cheng, G. Cristobal, M. Marquez and D. A. Weitz, *Angew. Chem., Int. Ed.*, 2006, **45**, 2556.
18 D. C. Duffy, J. C. McDonald, O. J. Schueller and G. M. Whitesides, *Anal. Chem.*, 1998, **70**, 4974.
19 Y. Xia and G. M. Whitesides, *Annu. Rev. Mater. Sci.*, 1998, **28**, 153.
20 S. H. Tan, N.-T. Nguyen, Y. C. Chua and T. G. Kang, *Biomicrofluidics*, 2010, **4**, 032204.
21 X. Niu, M. Zhang, S. Peng, W. Wen and P. Sheng, *Biomicrofluidics*, 2007, **1**, 44101.
22 B. Ahn, K. Lee, R. Louge and K. W. Oh, *Biomicrofluidics*, 2009, **3**, 44102.
23 V. Cristini and Y.-C. Tan, *Lab Chip*, 2004, **4**, 257.
24 B. Ahn, K. Lee, R. Panchapakesan and K. W. Oh, *Biomicrofluidics*, 2011, **5**, 024113.
25 F. Guo, X.-H. Ji, K. Liu, R.-X. He, L.-B. Zhao, Z.-X. Guo, W. Liu, S.-S. Guo and X.-Z. Zhao, *Appl. Phys. Lett.*, 2010, **96**, 193701.
26 M. Z. Bazant and T. M. Squires, *Phys. Rev. Lett.*, 2004, **92**, 066101.
27 M. E. Leunissen, A. van Blaaderen, A. D. Hollingsworth, M. T. Sullivan and P. M. Chaikin, *Proc. Natl. Acad. Sci. U. S. A.*, 2007, **104**, 2585.
28 W. D. Ristenpart, J. Bird, A. Belmonte, F. Dollar and H. Stone, *Nature*, 2009, **461**, 377.
29 L. Rao, B. Cai, X.-L. Yu, S.-S. Guo, W. Liu and X.-Z. Zhao, *AIP Adv.*, 2015, **5**, 057134.
30 L. Rao, B. Cai, J. Wang, Q. Meng, C. Ma, Z. He, J. Xu, Q. Huang, S. Li and Y. Cen, *Sens. Actuators, B*, 2015, **210**, 328.
31 S. H. Tan, F. Maes, B. Semin, J. Vrignon and J. C. Baret, *Sci. Rep.*, 2014, **4**, 4787.
32 S. H. Tan, B. Semin and J. C. Baret, *Lab Chip*, 2014, **14**, 1099.
33 E. Castro-Hernandez, P. García-Sánchez, S. H. Tan, A. M. Gañán-Calvo, J.-C. Baret and A. Ramos, *Microfluid. Nanofluid.*, 2015, **19**, 787.
34 E. Castro-Hernandez, P. Garcia-Sanchez, J. Alzaga-Gimeno, S. H. Tan, J. C. Baret and A. Ramos, *Biomicrofluidics*, 2016, **10**, 043504.
35 H. D. Xi, W. Guo, M. Leniart, Z. Z. Chong and S. H. Tan, *Lab Chip*, 2016, **16**, 2982.
36 K. Ahn, C. Kerbage, T. P. Hunt, R. Westervelt, D. R. Link and D. Weitz, *Appl. Phys. Lett.*, 2006, **88**, 24104.
37 H. A. Pohl, *Dielectrophoresis: the behavior of neutral matter in nonuniform electric fields*, Cambridge University Press, 1978.

38 R. Pethig, *Biomicrofluidics*, 2010, **4**, 22811.
39 J. J. Agresti, E. Antipov, A. R. Abate, K. Ahn, A. C. Rowat, J.-C. Baret, M. Marquez, A. M. Klibanov, A. D. Griffiths and D. A. Weitz, *Proc. Natl. Acad. Sci. U. S. A.*, 2010, **107**, 4004.
40 T. Beneyton, F. Coldren, J. C. Baret, A. D. Griffiths and V. Taly, *Analyst*, 2014, **139**, 3314.
41 T. Beneyton, I. P. M. Wijaya, P. Postros, M. Najah, P. Leblond, A. Couvent, E. Mayot, A. D. Griffiths and A. Drevelle, *Sci. Rep.*, 2016, **6**, 27223.
42 B. E. Debs, R. Utharala, I. V. Balyasnikova, A. D. Griffiths and C. A. Merten, *Proc. Natl. Acad. Sci. U. S. A.*, 2012, **109**, 11570.
43 P. Hammar, S. A. Angermayr, S. L. Sjostrom, J. Van Der Meer, K. J. Hellingwerf, E. P. Hudson and H. N. Joensson, *Biotechnol. Biofuels*, 2015, **8**, 193.
44 H. Hu, D. Eustace and C. A. Merten, *Lab Chip*, 2015, **15**, 3989.
45 M. Huang, Y. Bai, S. L. Sjostrom, B. M. Hallström, Z. Liu, D. Petranovic, M. Uhlén, H. N. Joensson, H. Andersson-Svahn and J. Nielsen, *Proc. Natl. Acad. Sci. U. S. A.*, 2015, **112**, E4689.
46 B. Kintses, C. Hein, M. F. Mohamed, M. Fischlechner, F. Courtois, C. Lainé and F. Hollfelder, *Chem. Biol.*, 2012, **19**, 1001.
47 M. Leman, F. Abouakil, A. D. Griffiths and P. Tabeling, *Lab Chip*, 2015, **15**, 753.
48 S. W. Lim, T. M. Tran and A. R. Abate, *PLoS One*, 2015, **10**, 1.
49 L. Mazutis, J. Gilbert, W. L. Ung, D. A. Weitz, A. D. Griffiths and J. A. Heyman, *Nat. Protoc.*, 2013, **8**, 870.
50 M. Najah, R. Calbrix, I. P. Mahendra-Wijaya, T. Beneyton, A. D. Griffiths and A. Drevelle, *Chem. Biol.*, 2014, **21**, 1722.
51 R. Ostafe, R. Prodanovic, W. L. Ung, D. A. Weitz and R. Fischer, *Biomicrofluidics*, 2014, **8**, 041102.
52 S. L. Sjostrom, Y. Bai, M. Huang, Z. Liu, J. Nielsen, H. N. Joensson and H. Andersson Svahn, *Lab Chip*, 2014, **14**, 806.
53 E. Zang, S. Brandes, M. Tovar, K. Martin, F. Mech, P. Horbert, T. Henkel, M. T. Figge and M. Roth, *Lab Chip*, 2013, **13**, 3707.
54 R. de Ruiter, A. M. Pit, V. M. de Oliveira, M. H. Duits, D. van den Ende and F. Mugele, *Lab Chip*, 2014, **14**, 883.
55 F. Saeki, J. Baum, H. Moon, J.-Y. Yoon, C. Kim and R. Garrell, *Polym. Mater.: Sci. Eng.*, 2001, **85**, 12.
56 W. C. Nelson and C.-J. C. Kim, *J. Adhes. Sci. Technol.*, 2012, **26**, 1747.
57 A. M. Pit, R. de Ruiter, A. Kumar, D. Wijnperlé, M. H. Duits and F. Mugele, *Biomicrofluidics*, 2015, **9**, 044116.
58 A. Sciambi and A. R. Abate, *Lab Chip*, 2014, **14**, 2605.
59 A. Sciambi and A. R. Abate, *Lab Chip*, 2015, **15**, 47.
60 D. J. Eastburn, Y. Huang, M. Pellegrino, A. Sciambi, L. J. Ptáček and A. R. Abate, *Nucleic Acids Res.*, 2015, **43**, e86.
61 B. Watson, J. Friend and L. Yeo, *Sens. Actuators, A*, 2009, **152**, 219.
62 L. Y. Yeo and J. R. Friend, *Annu. Rev. Fluid Mech.*, 2014, **46**, 379.
63 X. Ding, P. Li, S.-C. S. Lin, Z. S. Stratton, N. Nama, F. Guo, D. Slotcavage, X. Mao, J. Shi and F. Costanzo, *Lab Chip*, 2013, **13**, 3626.
64 F. Z. Bi and B. P. Barber, *IEEE Microwave Magazine*, 2008, vol. 5, p. 65.
65 W. Nyborg, *Phys. Acoust.*, 1965, **2B**, 1415.
66 K. Yosioka and Y. Kawasima, *Acta Acust. Acust.*, 1955, **5**, 167.
67 R. F. Milsom, N. Reilly and M. Redwood, *IEEE Trans. Sonics Ultrason.*, 1977, **24**, 147.
68 W.-K. Tseng, J.-L. Lin, W.-C. Sung, S.-H. Chen and G.-B. Lee, *J. Micromech. Microeng.*, 2006, **16**, 539.
69 G. Destgeer, S. Im, B. Hang Ha, J. Ho Jung, M. Ahmad Ansari and H. Jin Sung, *Appl. Phys. Lett.*, 2014, **104**, 023506.
70 R. J. Shilton, M. Travagliati, F. Beltram and M. Cecchini, *Appl. Phys. Lett.*, 2014, **105**, 074106.
71 Z. Ma, D. J. Collins and Y. Ai, *Anal. Chem.*, 2016, **88**, 5316.
72 G. Destgeer, B. H. Ha, J. H. Jung and H. J. Sung, *Lab Chip*, 2014, **14**, 4665.
73 G. Destgeer, K. H. Lee, J. H. Jung, A. Alazzam and H. J. Sung, *Lab Chip*, 2013, **13**, 4210.
74 D. J. Collins, A. Neild and Y. Ai, *Lab Chip*, 2016, **16**, 471.
75 D. J. Collins, Z. Ma and Y. Ai, *Anal. Chem.*, 2016, **88**, 5513.
76 M. Sesen, T. Alan and A. Neild, *Lab Chip*, 2015, **15**, 3030.
77 J. Lighthill, *J. Sound. Vib.*, 1978, **61**, 391.
78 M. B. Dentry, L. Y. Yeo and J. R. Friend, *Phys. Rev. E: Stat., Nonlinear, Soft Matter Phys.*, 2014, **89**, 013203.
79 V. Skowronek, R. W. Rambach, L. Schmid, K. Haase and T. Franke, *Anal. Chem.*, 2013, **85**, 9955.
80 T. Franke, A. R. Abate, D. A. Weitz and A. Wixforth, *Lab Chip*, 2009, **9**, 2625.
81 L. Schmid, D. A. Weitz and T. Franke, *Lab Chip*, 2014, **14**, 3710.
82 Y. Ai and B. L. Marrone, *Microfluid. Nanofluid.*, 2012, **13**, 715.
83 P. Brunet, M. Baudoin, O. B. Matar and F. Zoueshtiagh, *Phys. Rev. E: Stat., Nonlinear, Soft Matter Phys.*, 2010, **81**, 036315.
84 D. J. Collins, T. Alan, K. Helmerson and A. Neild, *Lab Chip*, 2013, **13**, 3225.
85 L. Schmid and T. Franke, *Lab Chip*, 2013, **13**, 1691.
86 J. Shi, S. Yazdi, S. C. Lin, X. Ding, I. K. Chiang, K. Sharp and T. J. Huang, *Lab Chip*, 2011, **11**, 2319.
87 J. Guo, Y. Kang and Y. Ai, *J. Colloid Interface Sci.*, 2015, **455**, 203.
88 L. Johansson, F. Nikolajeff, S. Johansson and S. Thorslund, *Anal. Chem.*, 2009, **81**, 5188.
89 J. Shi, D. Ahmed, X. Mao, S. C. Lin, A. Lawit and T. J. Huang, *Lab Chip*, 2009, **9**, 2890.
90 X. Ding, J. Shi, S. C. Lin, S. Yazdi, B. Kiraly and T. J. Huang, *Lab Chip*, 2012, **12**, 2491.
91 Z. Ma, J. Guo, Y. J. Liu and Y. Ai, *Nanoscale*, 2015, **7**, 14047.
92 J. Shi, H. Huang, Z. Stratton, Y. Huang and T. J. Huang, *Lab Chip*, 2009, **9**, 3354.
93 Y. Ai, C. K. Sanders and B. L. Marrone, *Anal. Chem.*, 2013, **85**, 9126.

94 X. Ding, Z. Peng, S.-C. S. Lin, M. Geri, S. Li, P. Li, Y. Chen, M. Dao, S. Suresh and T. J. Huang, *Proc. Natl. Acad. Sci. U. S. A.*, 2014, **111**, 12992.
95 P. Li, Z. Mao, Z. Peng, L. Zhou, Y. Chen, P.-H. Huang, C. I. Truica, J. J. Drabick, W. S. El-Deiry, M. Dao, S. Suresh and T. J. Huang, *Proc. Natl. Acad. Sci. U. S. A.*, 2015, **112**, 4970.
96 Z. Ma, A. Teo, S. Tan, Y. Ai and N.-T. Nguyen, *Micromachines*, 2016, **7**, 216.
97 J. Nam, H. Lim, C. Kim, J. Yoon Kang and S. Shin, *Biomicrofluidics*, 2012, **6**, 24120.
98 S. X. Li, X. Y. Ding, F. Guo, Y. C. Chen, M. I. Lapsley, S. C. S. Lin, L. Wang, J. P. McCoy, C. E. Cameron and T. J. Huang, *Anal. Chem.*, 2013, **85**, 5468.
99 M. Wiklund, C. Gunther, R. Lemor, M. Jager, G. Fuhr and H. M. Hertz, *Lab Chip*, 2006, **6**, 1537.
100 Z. Z. Chong, S. B. Tor, N. H. Loh, T. N. Wong, A. M. Ganan-Calvo, S. H. Tan and N. T. Nguyen, *Lab Chip*, 2015, **15**, 996.
101 T. Laurell, F. Petersson and A. Nilsson, *Chem. Soc. Rev.*, 2007, **36**, 492.
102 F. Petersson, A. Nilsson, C. Holm, H. Jonsson and T. Laurell, *Lab Chip*, 2005, **5**, 20.
103 I. Leibacher, P. Reichert and J. Dual, *Lab Chip*, 2015, **15**, 2896.
104 C. Lee, J. Lee, H. H. Kim, S. Y. Teh, A. Lee, I. Y. Chung, J. Y. Park and K. K. Shung, *Lab Chip*, 2012, **12**, 2736.
105 L. J. Thomas III, B. Barzilai, J. E. Perez, B. E. Sobel, S. A. Wickline and J. G. Miller, *IEEE Trans. Ultrason. Ferroelectr. Freq. Control*, 1989, **36**, 466.
106 L. Chen and R. B. Fair, *Microfluid. Nanofluid.*, 2015, **19**, 1349.
107 D. J. Shin and T. H. Wang, *Ann. Biomed. Eng.*, 2014, **42**, 2289.
108 M. Kuhnemund, D. Witters, M. Nilsson and J. Lammertyn, *Lab Chip*, 2014, **14**, 2983.
109 A. Chen, T. Byvank, W. J. Chang, A. Bharde, G. Vieira, B. L. Miller, J. J. Chalmers, R. Bashir and R. Sooryakumar, *Lab Chip*, 2013, **13**, 1172.
110 K. Raj, B. Moskowitz and R. Casciari, *J. Magn. Magn. Mater.*, 1995, **149**, 174.
111 M. A. Gijs, *Microfluid. Nanofluid.*, 2004, **1**, 22.
112 C. A. Heid, J. Stevens, K. J. Livak and P. M. Williams, *Genome Res.*, 1996, **6**, 986.
113 C. Zhang, Z. Zhao, N. A. A. Rahim, D. van Noort and H. Yu, *Lab Chip*, 2009, **9**, 3185.
114 Y. Jo, F. Shen, Y. K. Hahn, J. H. Park and J. K. Park, *Micromachines*, 2016, **7**, 56.
115 E. Surenjav, C. Priest, S. Herminghaus and R. Seemann, *Lab Chip*, 2009, **9**, 325.
116 S. H. Tan, N. T. Nguyen, L. Yobas and T. G. Kang, *J. Micromech. Microeng.*, 2010, **20**, 45004.
117 S. H. Tan and N. T. Nguyen, *Phys. Rev. E: Stat., Nonlinear, Soft Matter Phys.*, 2011, **84**, 036317.
118 J. Zhang, S. Yan, D. Yuan, Q. Zhao, S. H. Tan, N.-T. Nguyen and W. Li, *Lab Chip*, 2016, **16**, 3947.
119 G. Lin, L. Baraban, L. Han, D. Karnaushenko, D. Makarov, G. Cuniberti and O. G. Schmidt, *Sci. Rep.*, 2013, **3**, 2548.
120 T. Neuberger, B. Schöpf, H. Hofmann, M. Hofmann and B. Von Rechenberg, *J. Magn. Magn. Mater.*, 2005, **293**, 483.
121 C. Priest, S. Herminghaus and R. Seemann, *Appl. Phys. Lett.*, 2006, **89**, 134101.
122 T. Thorsen, R. W. Roberts, F. H. Arnold and S. R. Quake, *Phys. Rev. Lett.*, 2001, **86**, 4163.
123 T. Nisisako, T. Torii and T. Higuchi, *Lab Chip*, 2002, **2**, 24.
124 J. Liu, S.-H. Tan, Y. F. Yap, M. Y. Ng and N.-T. Nguyen, *Microfluid. Nanofluid.*, 2011, **11**, 177.
125 N. T. Nguyen, G. Zhu, Y. C. Chua, V. N. Phan and S. H. Tan, *Langmuir*, 2010, **26**, 12553.
126 B. Teste, N. Jamond, D. Ferraro, J.-L. Viovy and L. Malaquin, *Microfluid. Nanofluid.*, 2015, **19**, 141.
127 K. Zhang, Q. Liang, S. Ma, X. Mu, P. Hu, Y. Wang and G. Luo, *Lab Chip*, 2009, **9**, 2992.
128 M. Raffel, C. E. Willert, S. T. Wereley and J. Kompenhans, *Physical and Technical Background*, Springer, 2007.
129 Q. A. Pankhurst, J. Connolly, S. K. Jones and J. Dobson, *J. Phys. D: Appl. Phys.*, 2003, **36**, R167.
130 S. F. Medeiros, A. M. Santos, H. Fessi and A. Elaissari, *Int. J. Pharm.*, 2011, **403**, 139.
131 R. Moaddel, M. Marszall, F. Bighi, Q. Yang, X. Duan and I. Wainer, *Anal. Chem.*, 2007, **79**, 5414.
132 H. Li, Y. Wu, X. Wang, C. Zhu, T. Fu and Y. Ma, *RSC Adv.*, 2016, **6**, 778.
133 L. Wu, P. Chen, Y. Dong, X. Feng and B. F. Liu, *Biomed. Microdevices*, 2013, **15**, 553.
134 P. Chen, X. Feng, R. Hu, J. Sun, W. Du and B.-F. Liu, *Anal. Chim. Acta*, 2010, **663**, 1.
135 P. Chen, X. Feng, J. Sun, Y. Wang, W. Du and B.-F. Liu, *Lab Chip*, 2010, **10**, 1472.
136 J. Sun, P. Chen, X. Feng, W. Du and B.-F. Liu, *Biosens. Bioelectron.*, 2011, **26**, 3413.
137 Z. Cao, F. Chen, N. Bao, H. He, P. Xu, S. Jana, S. Jung, H. Lian and C. Lu, *Lab Chip*, 2013, **13**, 171.
138 Y. Zhan, J. Wang, N. Bao and C. Lu, *Anal. Chem.*, 2009, **81**, 2027.
139 V. Doyeux, T. Podgorski, S. Peponas, M. Ismail and G. Coupier, *J. Fluid Mech.*, 2011, **674**, 359.
140 M. Srisa-Art, I. C. Bonzani, A. Williams, M. M. Stevens and J. B. Edel, *Analyst*, 2009, **134**, 2239.
141 G. Aubry, M. Zhan and H. Lu, *Lab Chip*, 2015, **15**, 1424.
142 J. Shemesh, A. Bransky, M. Khoury and S. Levenberg, *Biomed. Microdevices*, 2010, **12**, 907.
143 Q. Zhang, P. Zhang, Y. Su, C. Mou, T. Zhou, M. Yang, J. Xu and B. Ma, *Lab Chip*, 2014, **14**, 4599.
144 C. Neagu, J. Gardeniers, M. Elwenspoek and J. Kelly, *Electrochim. Acta*, 1997, **42**, 3367.
145 Q. Yu, J. M. Bauer, J. S. Moore and D. J. Beebe, *Appl. Phys. Lett.*, 2001, **78**, 2589.
146 J. W. Hong, V. Studer, G. Hang, W. F. Anderson and S. R. Quake, *Nat. Biotechnol.*, 2004, **22**, 435.
147 H. Takao, K. Miyamura, H. Ebi, M. Ashiki, K. Sawada and M. Ishida, *Sens. Actuators, A*, 2005, **119**, 468.
148 A. Terray, J. Oakey and D. W. Marr, *Science*, 2002, **296**, 1841.

149 T. Thorsen, S. J. Maerkl and S. R. Quake, *Science*, 2002, **298**, 580.
150 Z. Z. Chong, W. J. Sim, Z. Ting Yeo, K. Ho Li, S. Huan Ng, H. Xia, T. N. Wong, N. Hiang Loh, S. Beng Tor and S. Hwa Tan, *Micro Nanosyst.*, 2014, **6**, 232.
151 G. Lin, D. D. Karnaushenko, G. S. C. Bermúdez, O. G. Schmidt and D. Makarov, *Small*, 2016, 4553.
152 A. R. Abate and D. A. Weitz, *Appl. Phys. Lett.*, 2008, **92**, 243509.
153 S. Lee, W. Jeong and D. J. Beebe, *Lab Chip*, 2003, **3**, 164.
154 M. A. Unger, H.-P. Chou, T. Thorsen, A. Scherer and S. R. Quake, *Science*, 2000, **288**, 113.
155 C. L. Hansen, S. Classen, J. M. Berger and S. R. Quake, *J. Am. Chem. Soc.*, 2006, **128**, 3142.
156 S. Quake, *Electrophoresis*, 2002, **23**, 1531.
157 J. Liu, C. Hansen and S. R. Quake, *Anal. Chem.*, 2003, **75**, 4718.
158 Y. Chen, Y. Tian, Z. Xu, X. Wang, S. Yu and L. Dong, *Appl. Phys. Lett.*, 2016, **109**, 143510.
159 D. Yoon, J. Ito, T. Sekiguchi and S. Shoji, *Micromachines*, 2013, **4**, 197.
160 A. R. Abate, J. J. Agresti and D. A. Weitz, *Appl. Phys. Lett.*, 2010, **96**, 203509.
161 D. H. Yoon, D. Wakui, A. Nakahara, T. Sekiguchi and S. Shoji, *RSC Adv.*, 2015, **5**, 2070.
162 Z. Jiao, X. Huang, N.-T. Nguyen and P. Abgrall, *Microfluid. Nanofluid.*, 2007, **5**, 205.
163 N.-T. Nguyen and X. Huang, *Jpn. J. Appl. Phys.*, 2005, **44**, 1139.
164 R. Savino, R. Monti and G. Alterio, *Phys. Fluids*, 2001, **13**, 1513.
165 S. S. Murshed, S.-H. Tan and N.-T. Nguyen, *J. Phys. D: Appl. Phys.*, 2008, **41**, 085502.
166 S. S. Murshed, S. H. Tan, N. T. Nguyen, T. N. Wong and L. Yobas, *Microfluid. Nanofluid.*, 2009, **6**, 253.
167 S. H. Lee, S.-W. Kim, J. Y. Kang and C. H. Ahn, *Lab Chip*, 2008, **8**, 2121.
168 Y.-F. Yap, S.-H. Tan, N.-T. Nguyen, S. M. S. Murshed, T.-N. Wong and L. Yobas, *J. Phys. D: Appl. Phys.*, 2009, **42**, 065503.
169 F. Jousse, R. Farr, D. R. Link, M. J. Fuerstman and P. Garstecki, *Phys. Rev. E: Stat., Nonlinear, Soft Matter Phys.*, 2006, **74**, 036311.
170 T. H. Ting, Y. F. Yap, N.-T. Nguyen, T. N. Wong, J. C. K. Chai and L. Yobas, *Appl. Phys. Lett.*, 2006, **89**, 234101.
171 V. Miralles, A. Huerre, H. Williams, B. Fournié and M. C. Jullien, *Lab Chip*, 2015, **15**, 2133.
172 N.-T. Nguyen, T.-H. Ting, Y.-F. Yap, T.-N. Wong, J. C.-K. Chai, W.-L. Ong, J. Zhou, S.-H. Tan and L. Yobas, *Appl. Phys. Lett.*, 2007, **91**, 084102.
173 S.-H. Tan, S. S. Murshed, N.-T. Nguyen, T. N. Wong and L. Yobas, *J. Phys. D: Appl. Phys.*, 2008, **41**, 165501.
174 J.-P. Delville, M. R. de Saint Vincent, R. D. Schroll, B. Issenmann, D. Lasseux, W. W. Zhang and E. Brasselet, *J. Opt. A: Pure Appl. Opt.*, 2009, **11**, 034015.
175 C. W. Tsao, Y. J. Lin, P. Y. Chen, Y. L. Yang and S. H. Tan, *Analyst*, 2016, **141**, 4973.
176 E. Verneuil, M. Cordero, F. Gallaire and C. N. Baroud, *Langmuir*, 2009, **25**, 5127.
177 C. N. Baroud, J.-P. Delville, F. Gallaire and R. Wunenburger, *Phys. Rev. E: Stat., Nonlinear, Soft Matter Phys.*, 2007, **75**, 046302.
178 B. Berge, O. Konovalov, J. Lajzerowicz, A. Renault, J. Rieu, M. Vallade, J. Als-Nielsen, G. Grubel and J. Legrand, *Phys. Rev. Lett.*, 1994, **73**, 1652.
179 E. Sloutskin, C. D. Bain, B. M. Ocko and M. Deutsch, *Faraday Discuss.*, 2005, **129**, 339.
180 J.-C. Baret, *Lab Chip*, 2012, **12**, 422.
181 F. Gallaire, C. N. Baroud and J.-P. Delville, *Heat Technol.*, 2008, **26**, 161.
182 M. Robert de Saint Vincent, R. Wunenburger and J.-P. Delville, *Appl. Phys. Lett.*, 2008, **92**, 154105.
183 K. D. Barton and R. S. Subramanian, *J. Colloid Interface Sci.*, 1989, **133**, 211.
184 Y. K. Bratukhin, K. Kostarev, A. Viviani and A. Zuev, *Exp. Fluids*, 2005, **38**, 594.
185 J. P. Gordon, R. C. C. Leite, R. S. Moore, S. P. S. Porto and J. R. Whinnery, *J. Appl. Phys.*, 1965, **36**, 3.
186 E. Fradet, C. McDougall, P. Abbyad, R. Dangla, D. McGloin and C. N. Baroud, *Lab Chip*, 2011, **11**, 4228.
187 R. Dangla, S. Lee and C. N. Baroud, *Phys. Rev. Lett.*, 2011, **107**, 124501.